

PASSDESIGN.RU



ЭЛЕКТРОННЫЙ ЖУРНАЛ  
КАЛИБРОВОЧНОЕ БЮРО

ВЫПУСК 7

Разработка и внедрение  
обучающих систем для  
подготовки студентов ВУЗов, ССУЗов  
и повышения квалификации кадров

# SiKE

SOFTWARE



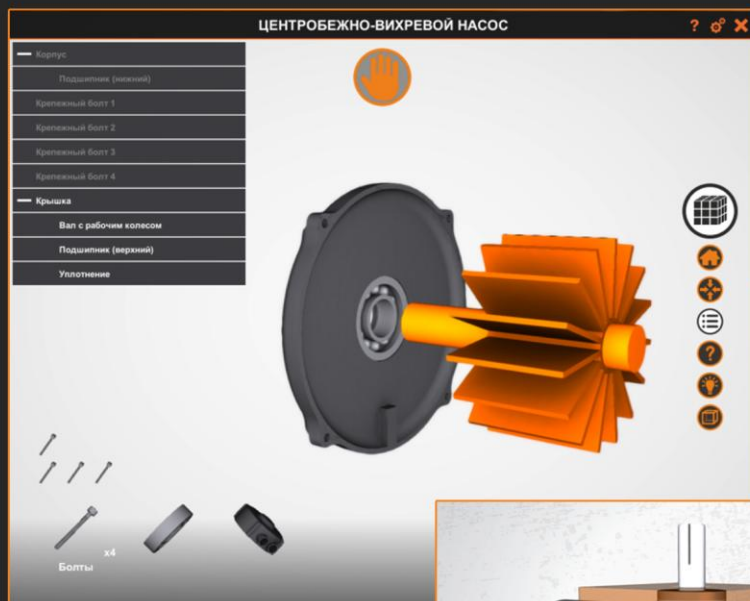
## МЫ ПРЕДЛАГАЕМ ГОТОВЫЕ РЕШЕНИЯ

3D АТЛАСЫ ОБОРУДОВАНИЯ  
3D СБОРКА/РАЗБОРКА  
АНИМАЦИОННЫЕ ФИЛЬМЫ  
ТРЕНАЖЕРЫ ИМИТАТОРЫ  
ЭЛЕКТРОННЫЕ КУРСЫ  
ЭЛЕКТРОННЫЕ ПЛАКАТЫ

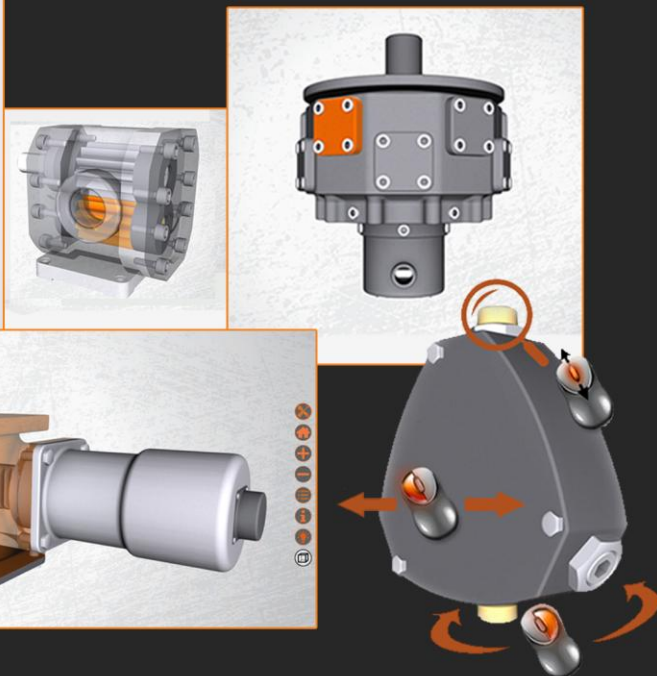
- Проблемы с текучкой кадров?
  - Неоправданные затраты на обучение?
  - Сотрудники долго и некачественно выполняют ремонт?

**КОМПАНИЯ SIKE ПРЕДЛАГАЕТ УНИКАЛЬНОЕ РЕШЕНИЕ**

## ОБУЧАЮЩАЯ СИСТЕМА «ВИРТУАЛЬНЫЙ МЕХАНИК»



Быстрая подготовка  
квалифицированного ремонтного  
и обслуживающего персонала на  
виртуальном оборудовании



Россия, г. Магнитогорск, 455023  
Тел.: 8 (3519) 22-22-44, 22-04-05  
E-mail: [info@sike.ru](mailto:info@sike.ru)  
Сайт: [sike.ru](http://sike.ru)  
Интернет-магазин: [shop.sike.ru](http://shop.sike.ru)

**«КАЛИБРОВОЧНОЕ БЮРО» Электронный научный журнал. Выпуск 7**

**Дата опубликования:** 28.08.2016.

Издается в авторской редакции

**УЧРЕДИТЕЛЬ И ИЗДАТЕЛЬ:** Кинзин Дмитрий Иванович.

**РЕДАКЦИОННАЯ КОЛЛЕГИЯ**

**Главный редактор:**

Д.И. Кинзин – кандидат технических наук, доцент.

**Технический редактор:**

С.А. Левандовский – кандидат технических наук, доцент.

**Адрес редакции:** 455000, г.Магнитогорск, ул. Ломоносова, 34, 8.

**Адрес в Интернет:** [www.passdesign.ru](http://www.passdesign.ru).

Издание зарегистрировано в Федеральной службе по надзору в сфере связи, информационных технологий и массовых коммуникаций и входит в базу данных Российского индекса научного цитирования (РИНЦ)

**Свидетельство о регистрации ЭЛ № ФС 77–51759 от 23.11.2012**

**ISSN 2308-6440**

© Кинзин Дмитрий Иванович

## СОДЕРЖАНИЕ

<b>Сортопрокатное производство</b> .....	5
<i>S. Spuzic</i> BASIC CONCEPTS IN ROLL PASS DESIGN.....	5
<i>S. Spuzic, K. Abhary, R. Ghomashchi</i> SOME ASPECTS OF DESIGN RATIONALISATION IN ROLLING TECHNOLOGY.....	7
<b>Листопрокатное производство</b> .....	32
<i>М.И. Румянцев, Д.Н. Чикишев, И.А. Разгулин</i> ОПЫТ КОНСТРУИРОВАНИЯ МОДЕЛИ ДЛЯ РАСЧЕТА МОМЕНТА ПРОКАТКИ НА ТОЛСТОЛИСТОВОМ СТАНЕ.....	32
<i>М.И. Румянцев, Д.Н. Чикишев, И.А. Разгулин</i> ОПЫТ КОНСТРУИРОВАНИЯ МОДЕЛИ ДЛЯ ПРОГНОЗА ТЕМПЕРАТУРЫ МЕТАЛ- ЛА ПРИ ПРОКАТКЕ НА ТОЛСТОЛИСТОВОМ СТАНЕ.....	36
<b>Сведения об авторах</b> .....	41

## BASIC CONCEPTS IN ROLL PASS DESIGN

The idea of roll pass design (RPD) is to design a series of [grooves](#) [1] within which the [rolled](#) [2] material will be deformed in order to achieve the desired [morphometry](#) [3] (geometry and dimensions) and [mechanical attributes](#) [4] of the finished product. The objective of RPD is to ensure that the product meets the desired [quality](#) [5] within constraints of the [mill](#) [6] and at minimum cost. The first approximation to RPD problem is to ensure practical manufacture of a long product with specified morphometric envelope and [mechanical](#) attributes [7].

A prerequisite for RPD analysis is to review the rolling mill layout and manufacturing parameters. Roll pass design can be viewed as a technique that results in producing the following documentation.

1. Product specification, that is, nominal features and tolerances for morphometry and the surface topography, as well as for the mechanical, chemical, [microstructural](#) [8] and other attributes of the product [material](#) [4]. The relevant information is usually available already (by means of international or [national](#) standards [9]), however, sometimes this is a matter for negotiation with the customers, resulting in the manufacturing norms for the agreed quality.
2. Specification of the above aspects for a series of transition objects – intermediate solids, including the initial feed. Manufacturing by rolling includes a number of discrete stages (sometimes over 50). The initial feed (usually a [cuboid](#) [10]) is deformed gradually, thus undergoing a decrease in cross-sectional area and an increase in the overall length during each stage (rolling pass). While the chemical composition does not change, the mechanical, surface and microstructure aspects will be substantially affected by the specifications of:
  - temperature gradient and its rate within and between each rolling pass;
  - deformation extent, gradient and rate within and between each pass.
 The relevant information (cross-sectional areas, elongations, rolling speeds, etc.) is usually summarized in so called ‘rolling schedules’ and complemented by means of technological instructions (documentation).
3. Deformation zone morphometry for each pass, by means of defining each in the sequence of roll grooves. This information complements the aspects in the point (2), with the ‘working’ diameters of the rolls the body of which is cut to create these grooves. The relevant information is summarized by means of groove drawings, including the positions of each groove relative to each other.
4. Tools (rolls) specification, that is, nominal features and tolerances for morphometry and surface topography, as well as for the mechanical, chemical, microstructural and other attributes of the tool material. This information includes the location of each roll in rolling mill, as well as the maximum and the minimum roll diameters, bearing in mind that each roll is redressed several times during its life to re-generate the initial groove morphometry. This is usually done after several rolling campaigns. Additional information includes the method of roll cooling, and in some cases, lubrication.
5. Complementary documentation, describing the feed preparation and heating techniques, as well as the finishing operations, after the rolling process itself is accomplished (such as the product cooling, straightening and cutting to the delivery lengths). This documentation includes information about the auxiliary equipment such as rolling tackle (guides and guards) which are necessary for guiding the rolled solid into each deformation zone.

Task (1) is straightforward, and the RPD engineers do not have much, if any, manoeuvring space in deciding the cutting lengths either. The major design analyses are related to the stages (2) to (5).

The diversity of combinations used by roll pass designers worldwide to define aspects in (2), (3) and (4) is mind provoking. It is understandable that differing rolling [mills](#) [11] use different

RPD systems for manufacturing similar products. This normally is a consequence of differences in [mill layouts](#) [12], stand configurations and other technical aspects. However, quite often the similar mills use very different RPD for rolling identical products. Useful RPD knowledge can be [extracted](#) [13] by [analysing](#) [14] this variety.

Additional important documentation consists of mill operation and maintenance records such as productivity, yield, tool life, maintenance indicators and the resource consumption.

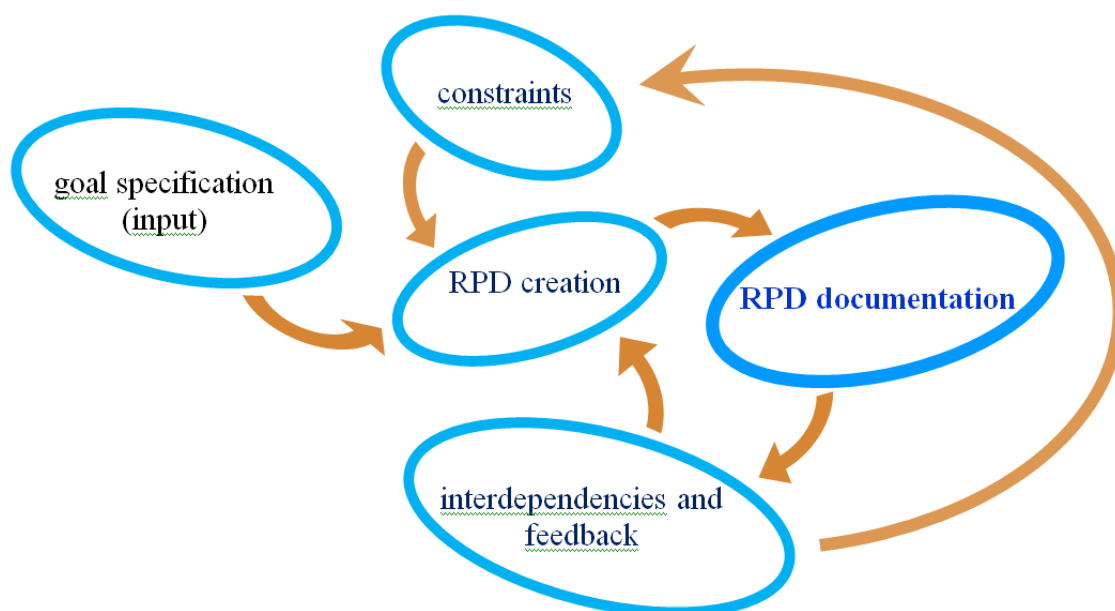
Optimisation of RPD, providing that process is void of catastrophic interruptions (such as appearance of cracks and tool fracture), can be evaluated on the basis of the following norms:

1 – yield; 2 – productivity; 3 – reliability; 4 – costs.

RPD in hot rolling mills is a principal factor that delimits all four listed norms.

Ideally, hot rolled material should plastically flow through a sequence of passes in such way to maintain an optimal level in all four above norms (indicators). More detailed analysis leads to the recognition of factors such as rolling pressure, friction, temperature, rolling and sliding velocity and tool life. All these variables are significantly affected by the phenomena embodied within the deformation zone which, in turn, is substantially influenced by the roll pass design.

There are number of different methodologies used in RPD, and the following algorithm presents a generic framework for accomplishing an RPD task.



## REFERENCES

1. <https://www.dropbox.com/s/6aaukdb4xeqqag7/Calibre.pdf?dl=0>
2. <http://www.doitpoms.ac.uk/tlplib/metal-forming-2/rolling.php>
3. <http://thelibraryofmanufacturing.com/imagesforming/metalrolling2a.jpg>
4. <https://dl.dropboxusercontent.com/u/14617698/050a.pdf>
5. <http://spuzic.yolasite.com/quality.php>
6. [http://s274.photobucket.com/user/sethmcs/media/degarmo\\_18-1.jpg.html](http://s274.photobucket.com/user/sethmcs/media/degarmo_18-1.jpg.html)
7. [https://en.wikipedia.org/wiki/List\\_of\\_materials\\_properties#Mechanical\\_properties](https://en.wikipedia.org/wiki/List_of_materials_properties#Mechanical_properties)
8. <http://www.msm.cam.ac.uk/phase-trans/abstracts/CP1b.html>
9. [http://www.passdesign.ru/index.php?option=com\\_content&view=article&id=84&Itemid=106](http://www.passdesign.ru/index.php?option=com_content&view=article&id=84&Itemid=106)
10. <http://www.amathsdictionaryforkids.com/qr/cimages/cuboid.gif>
11. <http://www.pertengineering.com/innovation/img/it03.jpg>
12. <http://www.rmttools.com/wp-content/gallery/sample-layout/sample-layout-of-Rolling-Mill-2.jpg>
13. <https://db.tt/NuNv9UM7>
14. [https://en.wikipedia.org/wiki/Multivariate\\_analysis](https://en.wikipedia.org/wiki/Multivariate_analysis)

**S. Spuzic, K. Abhary**

The University of South Australia

**R. Ghomashchi**

The University of Adelaide

This is the full version of an initial report presented at the International Conference Materials Innovation in Surface Engineering (MISE 2013) held in Adelaide 19th-21st November 2013.

An extract (20% from this report) was published in Materials Forum volume 37 – 2013 Edited by P.Howard, P.Huggett and D.Evans published by The Institute of Materials Engineering Australasia Ltd.

## **SOME ASPECTS OF DESIGN RATIONALISATION IN ROLLING TECHNOLOGY**

*Steel industry plays a critical role in climate change and hot rolling is a significant link in its technological chain. Further rationalisations in steel manufacture are important bearing in mind its strategic role and volume of consumed resources (e.g. ~ 90 t of fresh water for 1 t of a product). Thus it is important to control the tool (roll) performance and optimise roll pass design (RPD) including the selection of materials. RPD is a principal factor delimiting the process efficiency, product quality and the resource consumption. New avenues for improving RPD are to be found by extracting knowledge buried in the vast of industrial and published data bases. Basic idea is that improvements in RPD can be identified by propitious mathematical translations that enhance analyses of rolling series. Examples of analytical functions are introduced along with their use in RPD. Furthermore, a variety of methods for testing and comparing roll materials, used to complement and validate RPD is discussed. Along with reviewing some critical aspects of presented methods a lack of information about simulating the potential consequences of hot impact damage of rolls is addressed. A concept and a prototype of such a method are presented including the results of pilot tests conducted to evaluate this approach.*

### **1. INTRODUCTION**

The increasing evidence of global warming and the resource decline prompt for further rationalizations in large systems such as steel industry. In addition to environmental pollution, the steel industry is a large consumer of fresh water (not to mention the fuel consumption). A conservative estimate [1] is that the water requirements include nearly 90 tonnes of fresh water for 1 tonne of a steel product. Australia alone produced in last two years over 10 million tonnes of steel, which corresponds to nearly 900 million tonnes of fresh water sent to sea. This is more than 40% of the Adelaide water consumption per year. Government of South Australia (“the driest state in the driest continent on earth”) has issued a document Water Proofing Adelaide (a strategy plan up to 2025), which, among the other, asks for industrial rationalisation in water consumption [2].

Foreseeable long-term global views imply expansion of the needs for steel products, hence the radical solutions such as cuts in steel industry are not feasible. On the contrary, steel industry is increasingly adopting scientific approaches for more efficient energy usage and less pollution [3]. Moreover, the vast majority of infrastructure, tools and other equipment in steel industry itself, and in rolling mills in particular, are made out of steel materials. Over 80% of the steel products have been at some stage processed by hot rolling at 900 to 1200°C [4]. This prompted the considerable research and development activities in scientific, engineering and other public domains [1-29].

The computer aided roll design, application of CNC machines for roll turning and computer integrated roll manufacturing have become well established technology. The roll pass design is becoming even more advanced due to the growing importance of thermo-mechanical processes such

as controlled rolling. To meet the challenge of the future, research in fields concerning material flow, roll wear, and process rationality must adopt the interdisciplinary strategies [5].

The above considerations sum up to a conclusion that the technological improvements in hot rolling are of vital importance. The hot-steel – cold-roll interface is a critical aspect in this process intrinsically dependent on the continuity of operations. Inasmuch as the interactions along this interface are controlled by the deformation zone, it is important to note that any instant of the process interruption causes enormous losses. Expressed in monetary terms, one hour of delay (stoppage) in a rolling mill production process costs about \$ 30,000.

This publication discusses some new aspects of optimisation of the deformation zone and process continuity in hot steel rolling. The current technology does not take a sufficient advantage of information accumulated by product and tool manufacturers and users. A key for further optimisation must be sought in the roll pass design (RPD), a principal factor delimiting the process efficiency, product quality and the resource consumption. New avenues for improving RPD are to be found by means of extracting knowledge covered up in the industrial and otherwise published data bases. Basic idea is that improvements in RPD can be identified by propitious mathematical translation and statistical analyses of rolling series. Examples of generic analytical functions are introduced along with their use in analysing rolling series. The function parameters include the deformation zone, process parameters and the material attributes defining both the products and the tools.

While the products are delimited by the customers, the remaining parameters are matter of design rationality.

Designer has to satisfy rather intriguing requirements. The tool performance will be challenged immediately from the point of view of whether it can withstand the extreme thermal and mechanical loading. Furthermore, there is a standard expectation that certain level of productivity (e.g. t/hour), as well as a specified minimum yield and quality should be achieved without any (or with a minimum) corrections to the initial design.

However the surface phenomena such as thermal shocks, stress corrosion, abrasion, adhesion and surface layer fatigue, gradually degrade the tool performance. The rate of this continuous decline determines the reliability of key tools – the rolls.

Assuming that the product is defined by the standard or contract specifications, the designer will focus on the tool and process parameters.

The problem of design can be expressed in mathematical terms, such as the Durham Matrix-Based Methodology [6]. For example, in the process of selecting of the tool material, designers select differing combination of attributes associated with the wide spectrum of material testing methods in order to specify the “appropriate roll grade”. Ideally, an engineering material can be defined by a matrix the numeric components of which represent specific attributes:

$$\begin{bmatrix} X_{11} & X_{12} & \cdots & X_{1n} \\ X_{21} & X_{22} & \cdots & X_{2n} \\ \vdots & \vdots & \ddots & \vdots \\ X_{m1} & X_{m2} & \cdots & X_{mn} \end{bmatrix} = A. \quad (1)$$

Row 1 in matrix  $A$  can be used to specify chemical analysis, row 2 mechanical and other physical attributes, row 3 the materialographic characteristics, row 4 the tool material processing attributes such as heat treatment parameters, and so on.

The above matrix needs to be extended by increasing the number of entries to incorporate the aspects of the deformation zone geometry (such as the groove dimensions, roll diameters) the rolling process dynamics (e.g. the rolling velocity, strain rate, and stress distribution) and the operation parameters (such as the count of passes and tool cooling characteristics).

At this point it is useful to acknowledge that the physics of the phenomena in the deformation zone is far from being sufficiently understood. Although the analytical techniques have been greatly enhanced by development of information processors (computers), the relevant physics is oversim-

plified. Issues in practical rolling processes, such as the prediction of the deformation zone geometry or the actual phenomena along the cold-tool-hot-steel interface remain insufficiently understood, and therefore require further research [7, 8].

On the other hand, the actual practice of rolling processes continues to outstrip our theoretical understanding of it; the academic research and the industrial applications remain detached. This misalignment is evident despite the fact that an increasing volume of data collected during the industrial rolling can be analysed using scientific methods within the real time due to the advances in computerised information processing. These records describing a spectrum of rolling passes present an information rich sample space [7, 8].

All entries listed in Eq (1) are customarily recorded in industrial systems (rolling mill technology departments), however, not necessarily organised in a form that can be ordered in the matrix described above. Operation and quality control accumulate a vast amount of data such as the product yield and quality, process productivity, tool life, energy consumption, etc. This class of entries can be organised in analogous fashion, thus rendering the matrices of class  $B$ . Clearly the entries need to be represented by quantitative variables.

The data acquisition and processing systems allow for exploring the relations between the matrices  $B$  and  $A$ . In mathematical terms, an appropriately defined and sufficiently large data base allows for defining the pertinent statistics and dependences between the above matrices.

The records describing a variety of rolling passes present an information rich sample space. This treatise explains how these data can be structured and analysed.

The question of defining the relevant entries (system attributes) for each of the above matrices  $A$  and  $B$  deserves the particular attention and will be discussed in the next section. The emphasis is on scrutinising selected attributes from the point of their urgency and hierarchy and proposing improved alternatives.

## 2. SYSTEM ATTRIBUTES

### 2.1. General Remarks

The matrices representing the physical core of rolling mill system – the rolling process (line) – need to be defined by a finite count  $C$  of entries. Inasmuch as it is useful to quantify as many aspects as possible, there is a logical incentive to reduce this complexity. More complexity requires larger samples in order to reach the satisfactory confidence limits in the estimates of the population statistics, or satisfactory statistical power.

This introduces the problem of optimising the complexity of the matrix design. Some aspects of the entry hierarchy and complexity will be discussed below.

### 2.2. Some Aspects of Plastic Deformation in Rolling

Various deterministic methods, such as finite element/difference modelling and slip-line-fields continue to be used in attempts to optimise the process within the deformation zone. In addition, applications of genetic algorithms in RPD are increasingly probed but still fall short of being efficiently employed in practical applications. It is important noting that the genetic algorithms substantially rely on the observations and measurements recorded in actual rolling processes [8].

Inasmuch as an extensive research is based on the study of the coefficient of friction in the deformation zone, this information is inferior from a point of view of the matrix (1) entry hierarchy. Another aspect that stretches beyond the rational perimeter of significance is the extent of plastic flow beyond the deformation zone. This flow belongs to phenomena such as the coefficients of backward and forward creep [7]. Notwithstanding the usefulness of these aspects in the future developments, the logics of parsimony implies that a priority should be given to understanding the entries that can be measured and be controlled in order to realise actual processes.

Hence, the deformation zone is sufficiently defined by the geometries of two subsequent calibres including the roll diameters. In practice, the relevant information is encoded using a variety of dimensioning systems. This makes it hard to compare the effects of differing groove geometries. For example, the geometry of the very first calibre in rolling sequence resembles a rectangle modi-

fied by rounded corners (fillets), and by various curvatures and inclinations introduced along its sides (Figure 1).

However, some dimensioning systems use a differing code, as shown in Figure 2. In order to prepare entries for matrix (1), the grooves need to be defined using a consistent system of generic parameters. This misalignment becomes more critical when preparing entries for intermediate and finishing grooves, as shown in Figures 3-5.

Mathematically speaking, there is a need to introduce a generic analytical function such that changing its parameters results in reproducing the broad range of curves in the Cartesian coordinate system. This problem is simplified for the grooves with two perpendicular axes of symmetry. In such cases, the analytic function needs to mimic the actual groove contour in the 1<sup>st</sup> quadrant only, as shown in Figure 3 [22].

The grooves with only one (vertical) axis of symmetry must be represented by two analytic functions. Several cases of such functions are shown in Figures 4 and 5 [29].

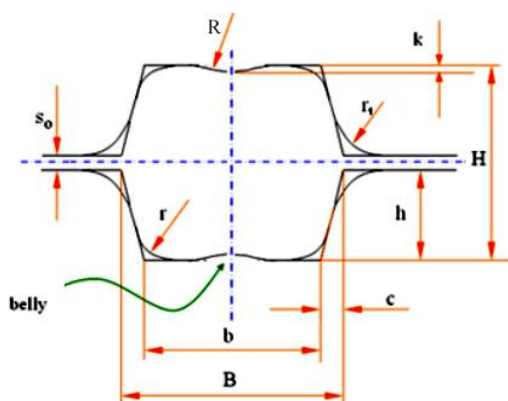


Fig. 1. A typical box groove

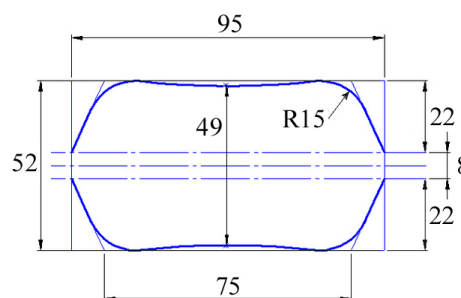


Fig. 2. An example of a traditional technical drawing of a box groove, where different dimensioning system is used compared to the case shown in Fig. 1.

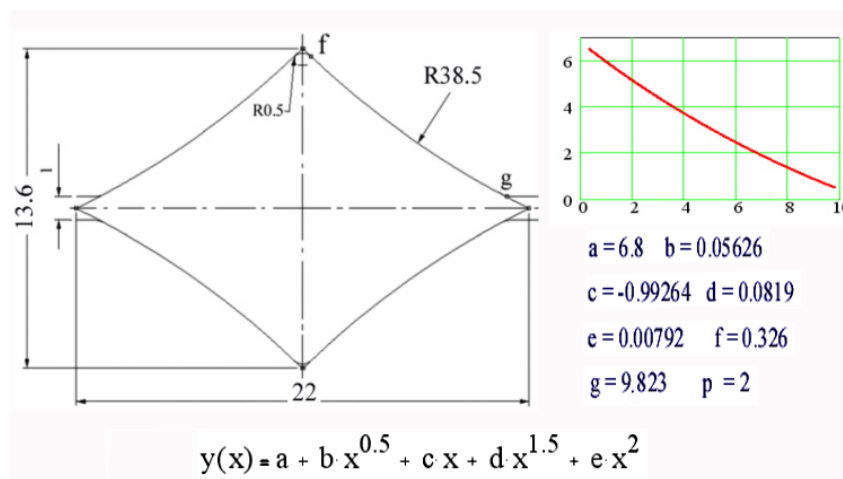


Fig. 3. Another example of traditional technical drawing of a groove with two axes of symmetry shown along a graph of its contour in the 1<sup>st</sup> quadrant of Cartesian coordinate system, and a generic analytical function defined by seven parameters (a,b,c,d,e,f and g)

One of design issues, of utmost importance for practical purposes, involves the confidence limits in estimates of groove dimensions. For example, if the bar lateral spreading is underestimated, the semi-industrial trials will result in an unavoidable overfill at the level of the roll gap in the subsequent passes. This imposes a need to reduce the width of the bar rolled at the preceding (initial) stages. This width is then most efficiently reduced by reducing the groove width (although

sometimes the minor corrections can be achieved by reducing the drafts, however, this usually results in overloading the finishing passes).

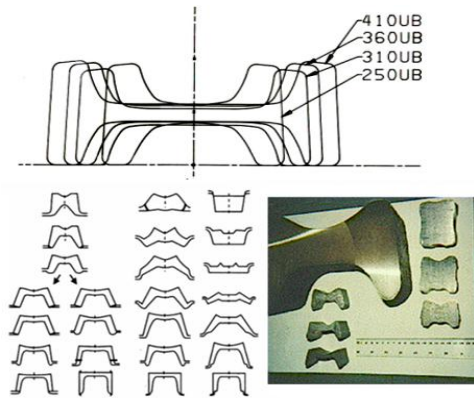


Fig. 4. Examples of grooves with one axis of symmetry

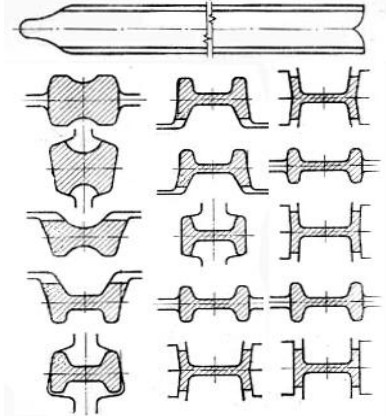


Fig. 5. Series of passes in rolling universal sections

In a situation when such correction is required to be made on already machined rolls, the only feasible way of reducing the groove width is by decreasing (losing) the roll diameter as indicated in Figures 6 and 7.

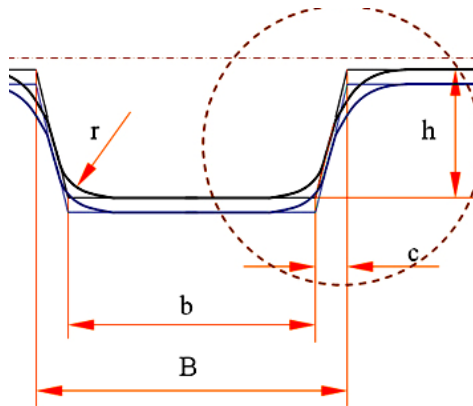


Fig. 6. Bottom half of a box calibre; the detail showing the decrease in the roll diameter and the groove width is shown in Fig. 7

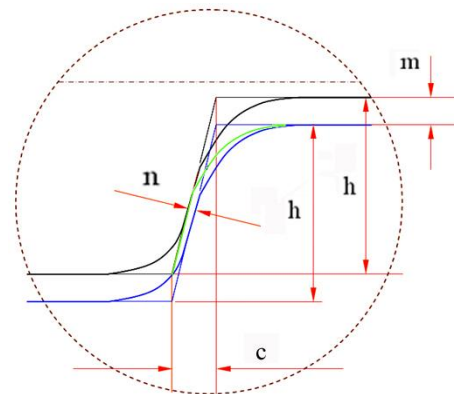


Fig. 7. In order to decrease the groove width by  $2n$ , the groove diameter of already turned rolls must be decreased by  $2m$

In order to avoid such costly corrections, and to ensure a stable rolling process, it is of paramount importance to make the reliable estimate of the groove width during the design stage. This problem can be reduced to defining the coordinates of the point  $g$  shown in Figures 3 and 8 [22].

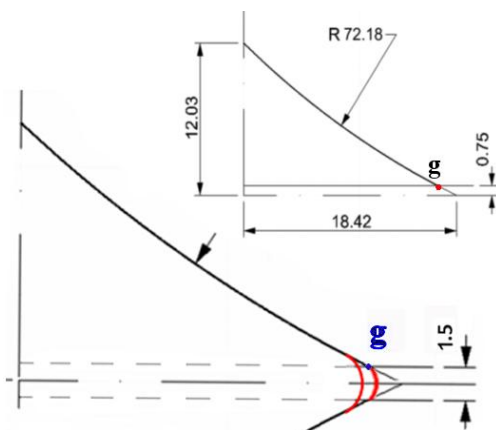


Fig. 8. The point  $g$  of the critical contact separation between the rolled steel and the roll groove surface

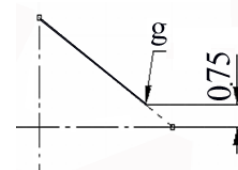


Fig. 9. A finishing square Groove represented in 1<sup>st</sup> Quadrant of the Cartesian Coordinate system

The advances in the FEM, finite difference or slip line analyses of the plastic flow in hot rolling are impressive. One disadvantage, however, is that for each change in any dimension on a groove contour, a new analysis has to be performed. A number of time consuming procedures (iterations) have to be conducted to arrive to a vicinity of the critical contact separation point.

With the models using the generic analytic functions, however, analyses related to the situation with the critical contact separation point can be solved directly using generic equation  $y(x)$  shown in Figure 3. The parameters for this equation are to be found by statistical analysis of industrial and otherwise published RPD data.

For example, by analysing the data base describing the series of two finishing passes in rolling square sections [21] (a rhombic, leader groove similar to the calibre shown in Fig. 8, and a square – final pass – shown in Fig. 9), an estimate can be made for a reliable position of point  $g$ .

As an example, the series shown by Vojkovsky et al [21], anticipates no curvature along the leader groove side for the designs aiming at finishing squares larger than  $k = 18.1 \text{ mm}$  (where  $k$  is the square side at the rolling temperatures of about  $900^\circ\text{C}$ ). However, statistical analyses of the parameters of generic functions conducted by Spuzic et al [22] indicate that it is beneficial to introduce a corresponding curvature at the leader (rhombic) pass, as defined by generic equation [22]

$$y(x) = 12.03 + 0.0585x^{0.5} - x + 0.0583x^{1.5} + 0.0045x^2. \quad (2)$$

This results in the dimensions for the leader groove as shown in Fig. 10.

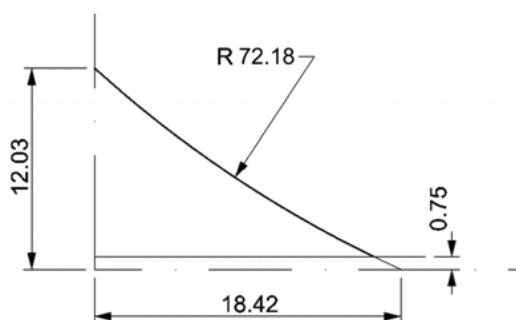


Fig. 10. Newly proposed design for the leader rhombic calibre for rolling square 19 mm

Statistical analysis of whole series using generic functions allows for calculating the maximum spread in the final calibre, i.e. the coordinates for the point  $g$  shown in Fig. 9, using the following correlation

$$x_g = -24.23 + 6.104 \ln(a_{romb}) + 52.367(d_{romb} \ln(a_{romb}))^2 + 118.214(e_{romb})^{0.5} + 0.653k. \quad (3)$$

The parameters  $b_{romb}$  and  $c_{romb}$  are omitted in Eq (3) since their values are constant (0.06 and -1.0, respectively) for the whole range in this series. Also, the value for  $y$  coordinate is constant  $y_g = 0.75 \text{ mm}$  [21].

According to Eq (3), the  $x$  coordinate for point  $g_{square}$ , in the case of using a modified leader calibre, is equal to  $x_g = 12.72 \text{ mm}$ , as opposed to 12.6 mm that was designed when using the original rhomb groove without the curved sides. The coefficient of determination is 0.9996, while F and t test are satisfactory at alpha risk of less than 0.1 and 0.03 respectively. The regression function defined by Eq (3) enables estimating the lateral spreading with the standard error of 0.055 mm. This in RPD practice means that first trials need to be conducted with  $x_g = 12.72 - 0.055 = 12.665 \text{ mm}$ .

The above example demonstrates that statistically significant information can be extracted from the data base collected from actual rolling practice.

More complex geometries require larger number of parameters. For example the class of grooves shown in Figures 4 and 5 have been currently defined by generic function having 25 parameters or more. Current research is focused on minimising this count to reduce the complexity of statistical analyses.

The above numerical relations need to be complemented by physical analyses based on the observations of plastic flow and microstructural phenomena. The computer based design can be further improved by physical simulations in a laboratory rolling mill, before entering the semi-industrial trials. Small-scale hot rolling mills are maintained by a range of research institutions, and recently some roll manufacturers develop this type of experimental facilities in order to validate and compare their roll grades. A compromise between the costs and reliability resulted in replacing hot steel by lead samples rolled at room temperatures. Extensive research and industrial practice provide ample evidence about the usefulness of laboratory experiments using lead models [8]. Figure 11 illustrates lead rolling, while Figure 12 shows comparisons of the results obtained by rolling lead vs. steel.

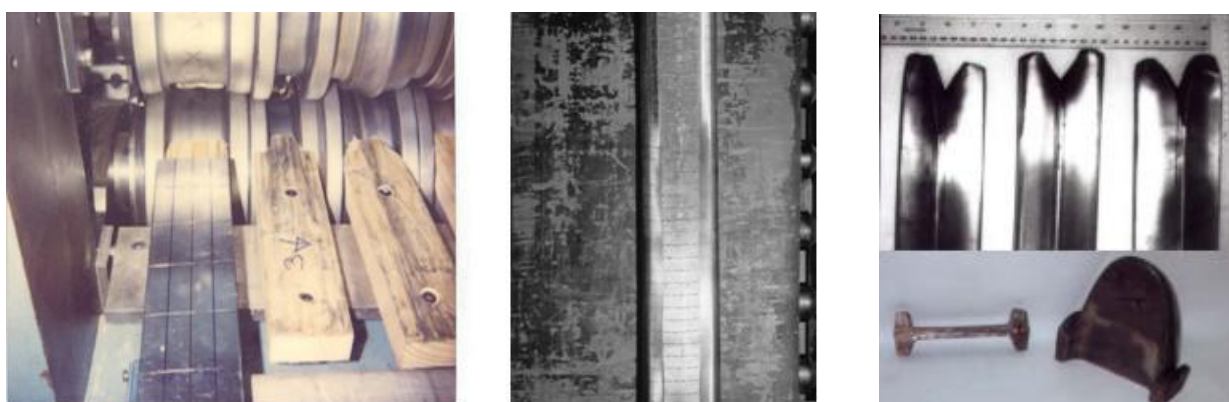


Fig. 11. The coordinate grid is imposed on the surface of lead samples rolled at a small-scale rolling mill; this method enables validation of FEM analysis of solid flow

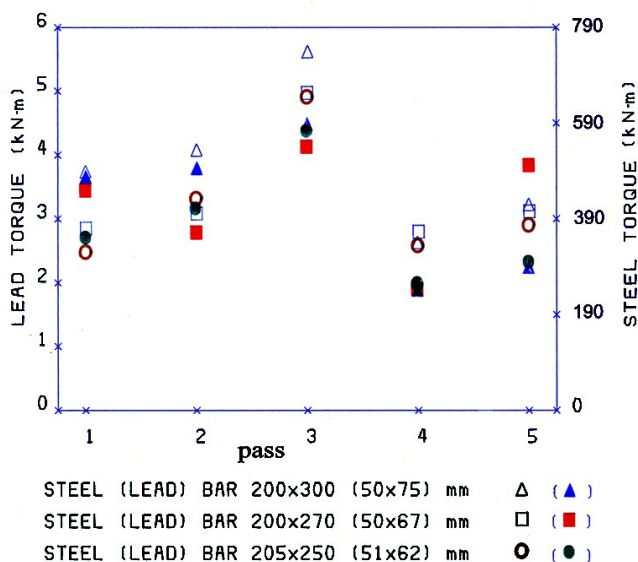


Fig. 12. Results of torque measurements obtained during industrial rolling of hot steel, and by means of the simulating the same rolling schedule by rolling lead; lead samples are rolled on small-scale laboratory rolling mill and at room temperatures

A design of the grooves for rolling long products has to be complemented by solving the problem of roll bite at the instant of the front end entry into the deformation zone. Generally, this problem arises at the initial stage of rolling sequence. In order to rationalise the overall process, the most intensive change in the cross-section geometry should be realised at the initial passes. Material

resistance to solid flow decreases rapidly with an increase in rolling temperature. This temperature has the highest values at the level of initial passes. Therefore the cross-section geometry should be rapidly modified at the level of initial passes, in order to transform the feed rectangular shape into a section that resembles the final geometry, as shown in Figures 4, 5 and 13.

However, the efficiency of this initial phase is limited by the affordable roll bite and the rolling velocity. The contemporary high-lift break-down mills are designed for withstanding high stresses and rolling torques, hence the mill power and strength are not the limiting factors.

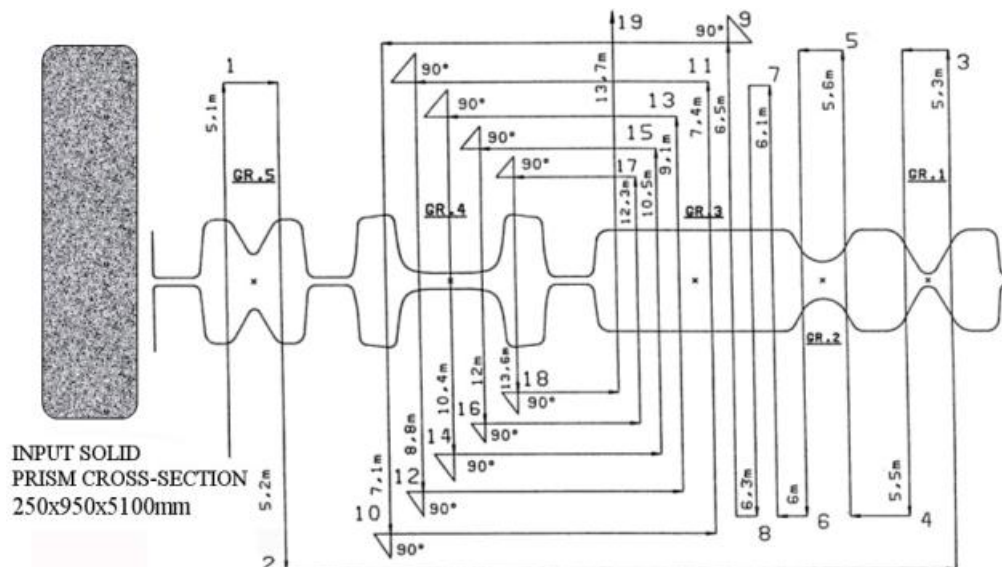


Fig. 13. Initial stage of rolling universal beams

The actual limitations are expressed by means of so-called maximum angle of bite  $\alpha$  which is related to the roll diameter  $D$  and vertical reduction  $\Delta h$  as illustrated by Eq (4) and Figure 14:

$$\cos \alpha = 1 - \frac{\Delta h}{D}. \tag{4}$$

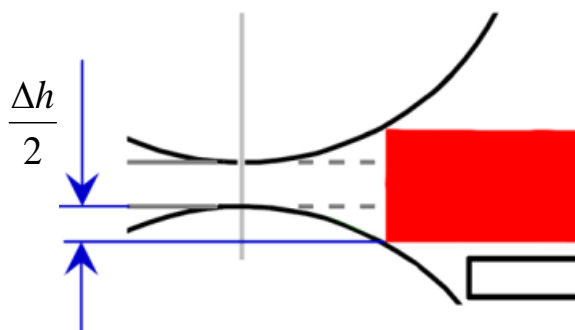


Fig. 14. Schematic of the initial contact between the front end of the rolled bar and the roll surface (in this case the front end angle is 90°)

This angle can be increased if  $\Delta h$  can be reduced at the instant of the first contact of the front end with roll surface [24]. However, when  $\alpha$  is increased, the actual reduction  $\Delta h$  can be radically increased once the deformation zone has been filled with the hot steel completely.

This can be achieved by introducing a chamfer at the bar ends as shown in Figure 15.

Experiments by rolling lead samples at room temperatures allow inferring that higher drafts can be achieved at an increased rolling velocity if there is a chamfer introduced at the front end of the rolled bar. Figure 16 shows the results of statistical analysis of rolling bars with differing angles of the front end chamfer. The alpha risk associated with the inferred trends is 0.15.

However, the roll pass design is not limited to the above discussed analyses of the deformation zone geometry and dynamics. Another important issue, substantially affecting the rolling

product quality and process efficiency as well as the sustainability of the whole system is related to the reliability of the principal tools – the rolls.

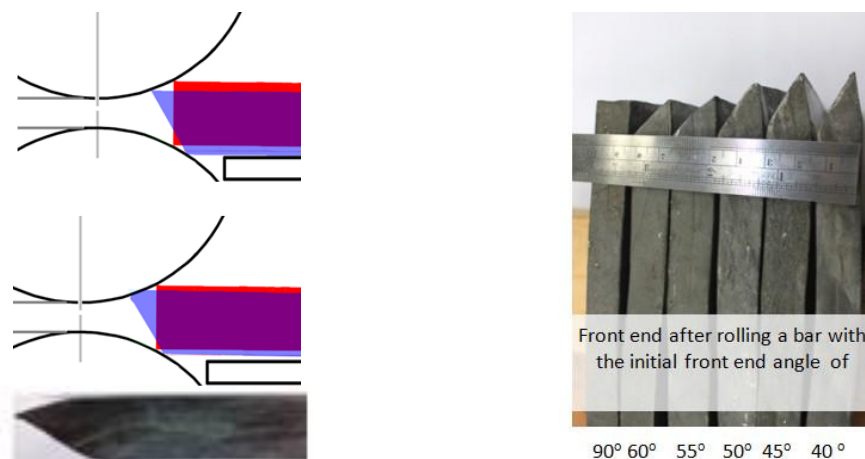


Fig. 15. (Top left) a sketch showing the initial points of contact when a chamfer of 50° is introduced; (bottom left) a photo of the chamfered lead sample after rolling; (right) front end shapes of rolled lead samples which had before rolling the chamfers at differing angles

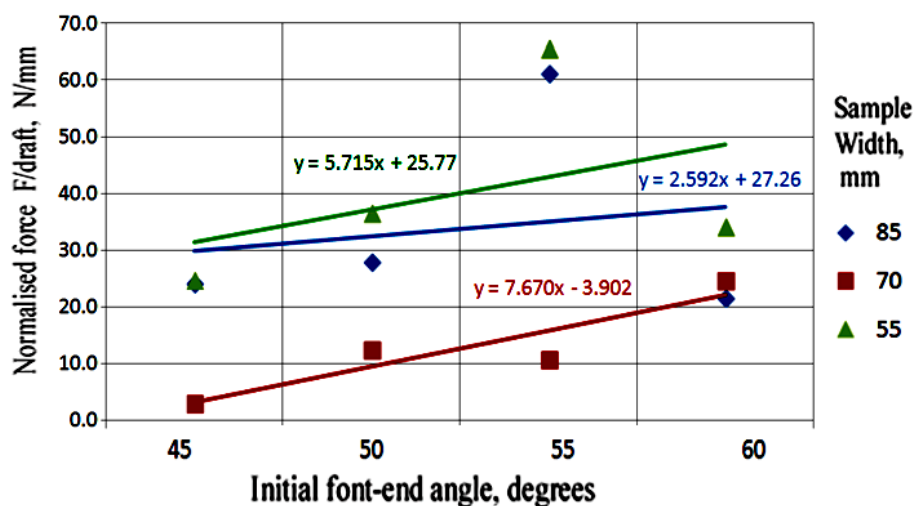


Fig. 16. Graph showing the increase of the horizontal force needed to push the lead sample into the deformation zone with increasing chamfer angle

### 2.3 Tool (Roll) Material Attributes

Designers routinely select the tool material from the assortment offered by specialised roll manufacturers.

Available specifications present the chemical composition (chemical analysis for Carbon and other alloying elements), mechanical attributes (hardness, tensile strength, notch impact test, etc) and additional data such as materialographic information. Roll suppliers base their presentation on a range of standardised testing methods [11-16]. In addition, most of roll manufacturers have developed their own quality control techniques and various technological tests aiming to simulate the roll exploitation conditions [17].

Figure 17 illustrates an overview of typical roll materials.

The concept of carbon equivalent is a classical example of attempts to reduce the complexity of the information describing the chemical analysis.

A roll pass design must first satisfy the criteria with regard to the bulk strength, thus providing the needed safety against the tool fracture. Further criteria, however, involve a more subtle, long term, issue of tool surface deterioration. This deterioration involves abrasion, adhesion, corrosion, ploughing, thermal and mechanical cracking as well as various combinations of the listed phenomena along with further modes of surface and subsurface damage, Figure 18-20 [9, 17-20, 25].

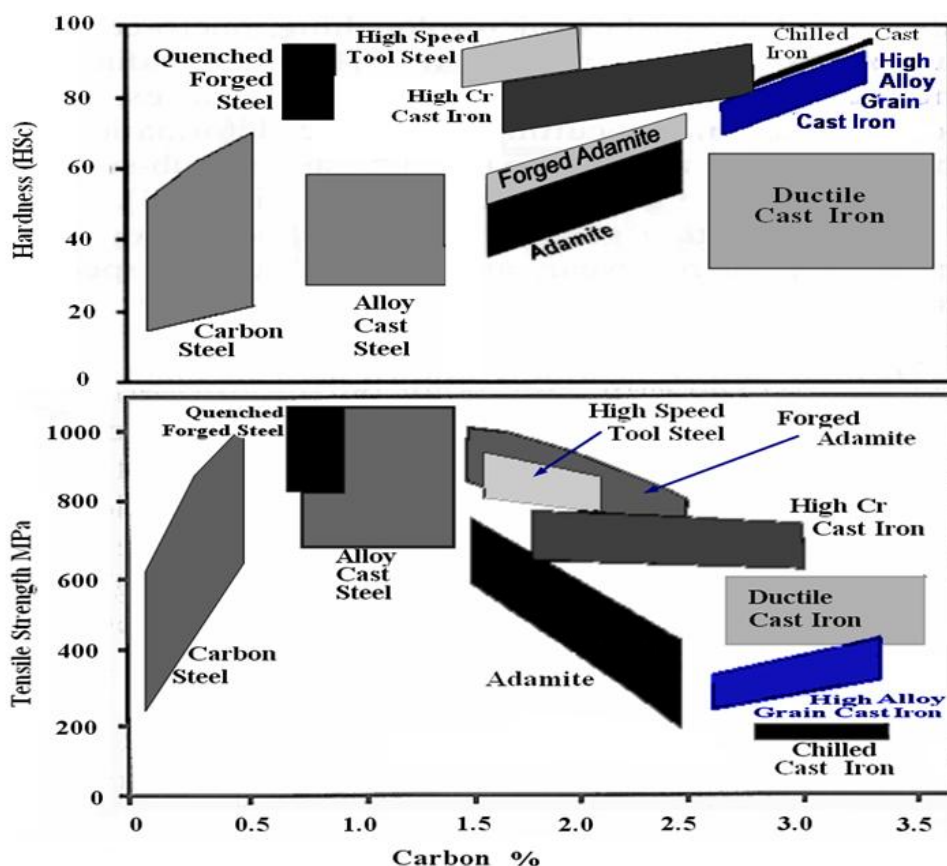


Fig. 17. Typical roll materials [25]

From the point of view of the rolling process designers, roll material is best defined by the attributes that are correlated directly to the tool performance. While the methods for measuring mechanical attributes, such as static and dynamic tests are well standardised, the simulation of the conditions encountered during hot rolling still represents a hard challenge. A variety of tests configurations were developed, however, these methods are limited to the reproduction of a specific aspect of a more complex real system. In general, the attributes evaluated are dependent on the applied tribological system. Bearing in mind the wide experimental conditions, the relative contribution of the wear modes can vary broadly [17, 19, 21].

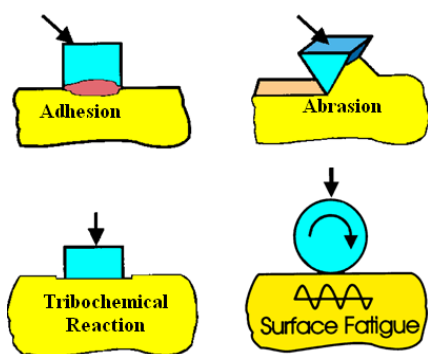


Fig. 18. Wear modes [25]



Fig. 19. Typical examples of roll surface wear

In most cases an individual hot wear test allows only to observe a difference in wear resistance between roll materials grades such as adamite, indefinite chill, high chromium irons and high speed steels [9, 17].

Although the significant number of authors use the so called “disc-on-disc” rolling-sliding tester [17, 19, 25], there are inconsistencies in the interpretations of the results. Namely, in this simulation illustrated in Fig 21, the wear rate ( $w$ ) is one of the most important criteria.

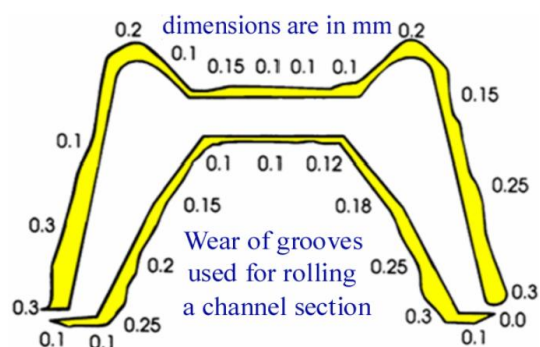


Fig. 20. Wear of the  $\varnothing 650$  mm rolls for 200 mm channel section; a consequence of continuous wear due to sliding of the hot steel along the groove surface [25]

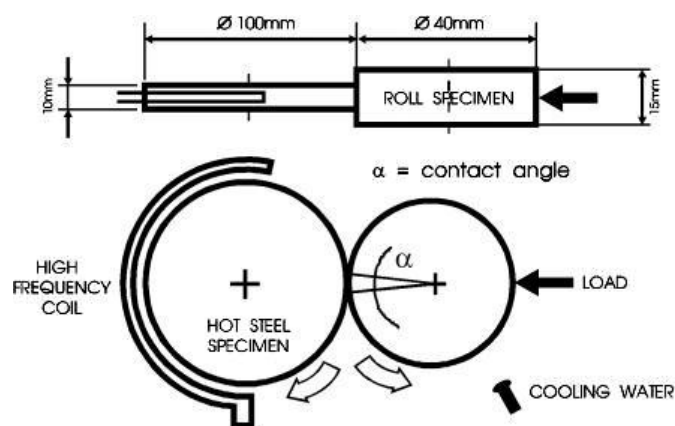


Fig. 21. Schematic of a disc-on-disc tester [17, 25]

However, a variety of norms have been used to measure hot roll wear:

1. the mass removed during wear,  $\Delta M$ ,
  2. the volume worn out,  $\Delta V$ , or
  3. the depth of the worn layer,  $\Delta R$ ,
- each of these norms being usually related to one of the following variables:
- a. the number of revolutions ( $N$ ),
  - b. sliding distance ( $L$ ) or
  - c. contact time ( $\tau$ ).

The particular suitability of the measure of wear is influenced by the motives of investigation. For example, the use of  $\Delta M$  would show the effects of differences in the density of roll materials on wear. In reality, the concern in rolling mill roll wear is not the worn mass or worn volume, but the wear depth. In particular, the radial wear,  $\Delta R$ , is of much concern. This term,  $\Delta R$ , can be defined in various ways [17].

A definition applied in real conditions met in a roll shop, describes the depth of the worn layer as the decrease in roll radius caused by both wear and subsequent machining. The surface microstructure is affected by thermomechanical stresses and diffusion processes. Further factors are surface and subsurface micro and macro cracks. The amount of radial machining has to be increased (by factor of 3 to 4) to return the surface layer to the original microstructure that was present before rolling. Such a definition of  $\Delta R$  is, however, inappropriate when the purpose of the test is to isolate abrasive mechanism from thermomechanical fatigue in a disc-on-disc laboratory simulation [17].

The following discussion is concerned with the denominator  $Q$  in the wear rate expression:

$$w = \Delta R / Q. \quad (5)$$

The terms under consideration for  $Q$  are:

1. number of revolutions,  $N$ , (used widely in examining rolling-sliding wear),
2. contact time  $\tau$  (a basic denominator in analysis of the process kinetic), and
3. sliding distance,  $L$ , (the variable of crucial importance in fundamental models of abrasion) [17].

1) The total number of revolutions (or collisions)  $N$  is clearly useful for the investigation of thermo-mechanical fatigue and related phenomena in rolling-sliding wear. A range of authors, use the number of revolutions to consider wear behaviour in rolling-sliding contact. However, it has been noted that the presence of sliding significantly affects not only abrasion, but also the fatigue mechanism. Clearly, depending on the sliding velocity employed, a solid of revolution can experience very different abrasive wear depth, even during a single rotation. It also appears that during the same single rotation and under constant sliding velocity, the wear depth of a solid of revolution will differ depending on the contact zone length. As shown in Fig. 22, it is obvious that disc (a) has

shorter contact zone length,  $s$ , than disc (b). Hence, given all other variables are constant, it follows that the wear depth of disc (a) will be less than that of disc (b) [17].

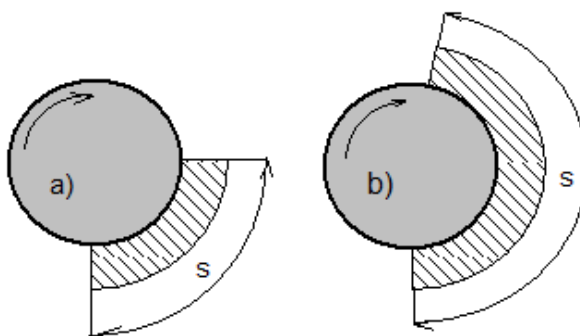


Fig. 22. Two cases of rolling-sliding contact, differing only with respect to contact zone length,  $s$  [17]

2) The contact time  $\tau$  is clearly useful in many considerations and is widely employed as a norm in presenting wear behaviour. However, contact time is functionally connected to variables such as sliding distance,  $L$ , sliding velocity,  $U$ , and the geometric parameters of deformation zone, ( $s$  and  $D$ ). If  $\tau$  is known, but the information on some of the above attributes is missing, the basic mechanical information is incomplete. For example, in a relatively short time a significant sliding distance can be experienced, depending on the sliding velocity and the deformation zone length. In other words, the functional relationship between the contact time and geometric and kinetic variables has to be taken into account, before any tribological conclusion or prediction can be made based on the obtained wear depth per unit of elapsed contact time.

3) In a situation where the abrasive wear dominates, the sliding distance  $L$  is one of the fundamental terms that should be directly involved in wear models. This sliding distance  $L$  in rolling-sliding contact can be calculated using the following equation:

$$L = N s \frac{U}{v}, \quad (6)$$

$N$  = total count of revolutions of the rotating solid for which  $L$  is calculated;

$s$  = contact zone length;

$U$  = difference between the tangential velocities of contacting solids engaged in rolling-sliding contact;

$v$  = peripheral velocity of the solid for which  $L$  is calculated.

Hence, Eq (5) becomes

$$w = \Delta R / L. \quad (7)$$

In the case of the deformation zone in rolling

$$s = \sqrt{0.5 D \Delta h}, \quad (8)$$

$D$  = roll diameter;

$\Delta h$  = vertical draft (se Fig 14).

In the case of disc-on-disc tester:

$$s = 1.6 \sqrt{\left( \frac{1 - \nu_1^2}{E_1} + \frac{1 - \nu_2^2}{E_2} \right) \frac{F}{b} \frac{D_1 D_2}{D_1 + D_2}}, \quad (9)$$

$\nu_{1,2}$  = Poisson's coefficient for the material of disc 1 and 2, respectively;

$E_{1,2}$  = Young's modulus for the material of disc 1 and 2, respectively;

$F$  = contact force acting in the direction connecting disc centres;

$b$  = contact width.

The above theoretical base allows for conceptualising useful physical experiments. However, any physical measurement will still involve effects of so-called random factors, the significance of which cannot be always sufficiently explained by statistics. Along with the statistical quantifications and inferences a better understanding of involved phenomena requires materialographic observations up to the level of scanning and transmission electron microscopy (SEM and TEM).

Experiments conducted by number of authors [9, 17-20] provide ample evidence about abrasive wear of the roll surface due to the rolling-sliding contact with hot steel surface covered by layers of hard oxides, Fig 23 and 24.

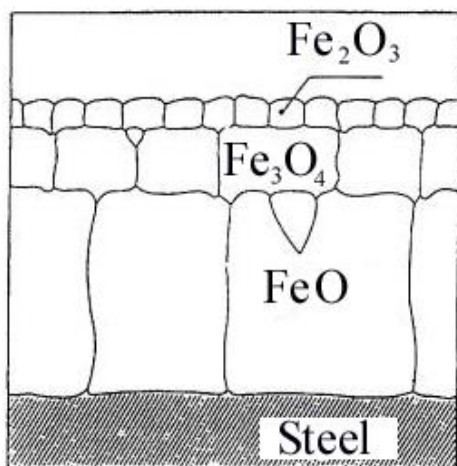


Fig. 23. Oxide layers on the surface of hot rolled steel [17]

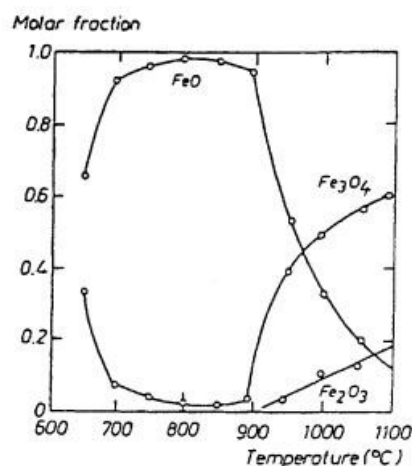


Fig. 24. Distribution of Fe-oxides (wustite FeO, magnetite Fe<sub>3</sub>O<sub>4</sub> and haematite Fe<sub>2</sub>O<sub>3</sub>) at rolling temperatures [17]

Typical results of the disc-on-disc test on the adamite roll material are shown in Figures 25, 26 and 27.

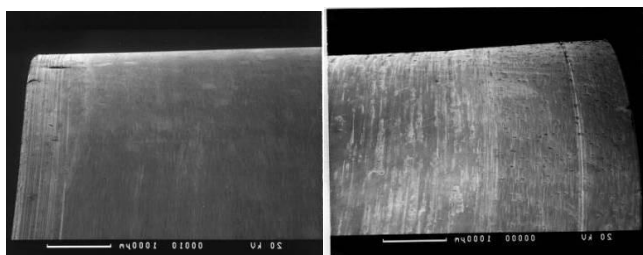


Fig. 25. Disc surface before and after wear test (rolling sliding contact with a hot steel disc heated to 900°C) [17]

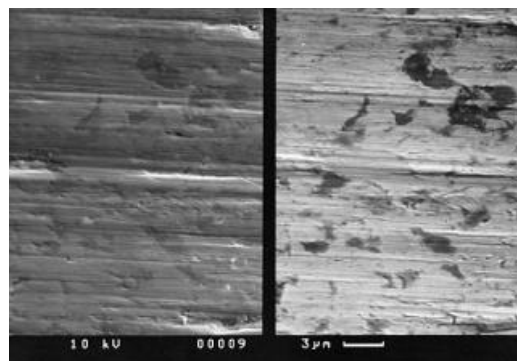


Fig. 26. Top view on the worn surface of the adamite roll sample; traces of abrasion are visible along with the patches of adhered oxides that are transferred from the hot steel surface; EDX analysis confirmed presence of iron oxides in the wear track cavities [17]

Profilometry enabled measurement of the wear depth  $\Delta R$  for a number of roll samples exposed to abrasion against a hot steel disc at elevated temperatures using differing forces, sliding velocities and temperatures. Results are shown in Fig 28 [17].

The above approach allowed for distinguishing the wear behaviour of two adamite roll materials (material “A” with 1.2% C and “B” having 1.8% C), Fig 29.

The disc-on-disc hot wear simulation has proven that the abrasive wear decreased by increase of carbon content i.e. the mean hardness via an increase of hard carbide fraction. SEM micrograph

in Fig 30 shows a high magnification of carbide particles protruding out of the wear track after exposure to rolling-sliding contact with hot steel (normal force  $F = 200N$ , hot steel disc temperature  $800^{\circ}C$ , sliding velocity  $U = 0.7m/s$ , material adamite B). Two examined roll materials, adamites of different carbon content, i.e. 1.2% C (sample A) and 1.8% C (sample B), are true representative of tools used in rolling mill. The roll specimens (discs  $\varnothing 40mm$ ) were cut of the peripheral locations of real rolls ( $\varnothing 1200mm$ ) [17].

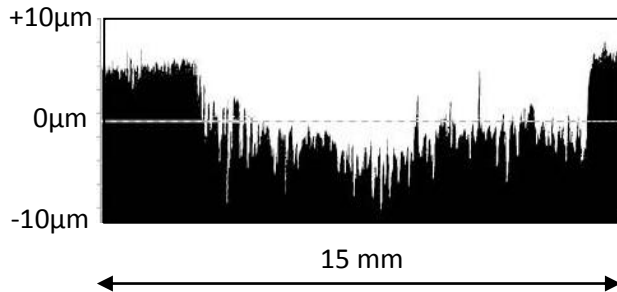


Fig. 27. Wear track of the sample shown in Fig 25; this run is performed using the sliding velocity of 0.7 m/s, contact force of 200 N and hot steel temperature of  $800^{\circ}C$  [17]

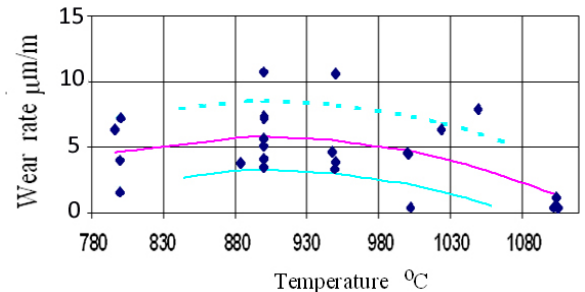


Fig. 28. The correlation between the wear rate of adamite roll material and the hot steel temperature; normal force  $F = 300N$ , sliding velocity  $U = 0.25m/s$ , coefficient of determination  $r^2 = 0.6$  [17, 18]

Significance of the abrasion mode due to the presence of hard Fe-oxides on the surface of hot rolled steel has prompted attempts to isolate this single wear mechanism by means of single scratch testing [26].

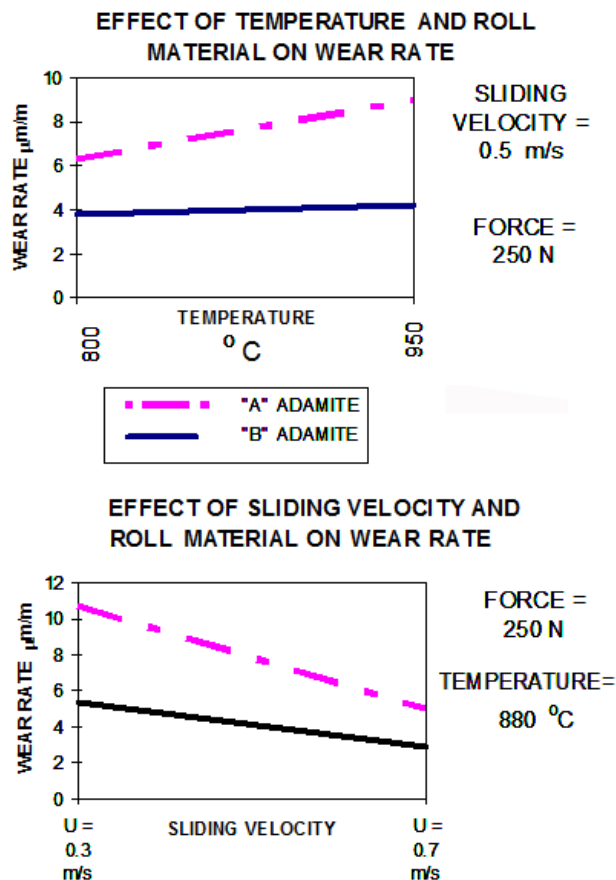


Fig. 29. Differing wear behaviour of adamite A (1.2% C) and adamite B (1.8% C); it is obvious that adamite A is more sensitive to the effects of both temperature (of the counter-body) and sliding velocity, and less resistant to high temperature abrasion, compared to material B [17]

This complementary method, scratch testing, has confirmed that adamite with the higher content of the carbon of 1.8% C (sample B), has better resistance to abrasion compared to adamite with 1.2% C (sample A). Figures 31 and 32 show how the microstructure of these two materials reacted on scratching. It is clear that the hard carbides, that occupied a larger fraction in the volume of adamite B, presented barriers to scratch propagation, Fig 31.

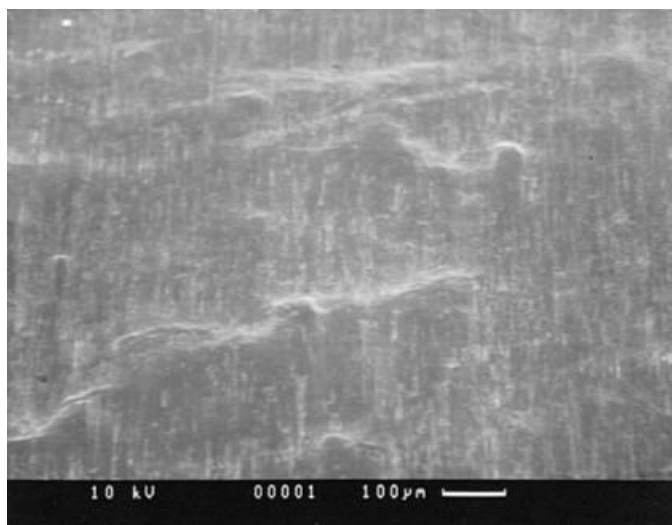


Fig. 30. SEM micrograph showing a high magnification of a carbide particles protruding out of the wear track after rolling-sliding wear run (normal force  $F = 300N$ , hot steel disc temperature  $1000^{\circ}C$ , sliding velocity  $U = 0.25m/s$ , material adamite B)

On the contrary, the microstructure of the softer material, adamite A, reacted by plastic deformation waves along the scratch walls, Figure 32.

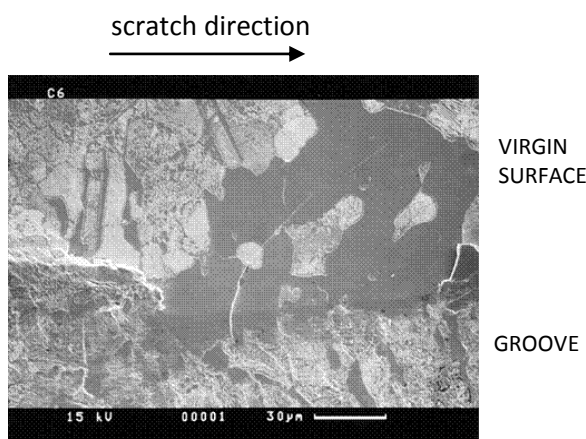


Fig. 31. Adamite "B" material (1.8 wt. % carbon; etched 2% Nital); SEM micrograph of a single scratch made on a polished surface [17, 26]

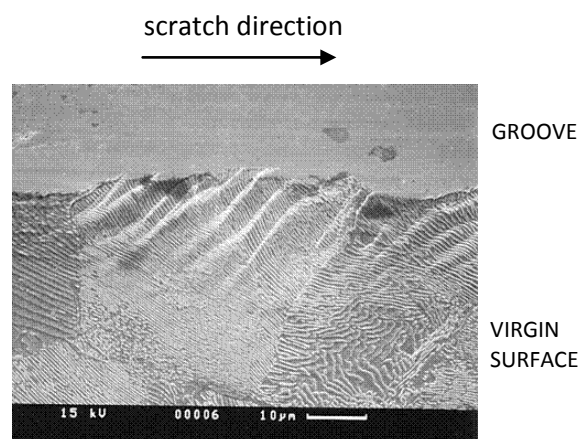


Fig. 32. Adamite "A" material (1.2% C); SEM micrographs of scratch edge morphology; etched 5% Nital, before scratching [17, 26]

In addition, evidence has been collected about the effect of surface bulk stress state on wear resistance. A special jig (Figure 33) was designed to create the desired stress state in bent beams. The purpose of this jig was to enable the scratching as well as the measurement and observation of the scratches in situ. A scratch tester equipped with normal and tangential force measurement was used to generate single scratches on a surface of the stressed samples. The scratching rate was 10 mm/min; a diamond indenter (cone with a tip radius of 0.2 mm) was used and loaded at a rate of 110 N/min. Scratch geometry was measured using computer controlled Taylor-Hobson Form Talysurf [17, 26].

The samples (plates 18x2.5x83mm) were exposed to various bulk stress states, within the range of elastic stresses. The induced bulk stress was perpendicular to both the normal scratching force and the longitudinal axis of the scratch. After the desired stress was achieved in surface layers

of the steel sample, the complete jig (with sample) was mounted on the working table of the scratch tester, and the sample surface was scratched by single penetration and transverse movement of the diamond indenter. Scratch topography was observed and scratch geometry measured both in situ and in relaxed state [17, 26].

It was observed that the scratches on surfaces under bulk tension were deeper compared to the scratches on surfaces under compression. In other words, the surface of steel was more resistant to abrasion in the presence of compression bulk stress state. The mechanistic explanation for this is straightforward, Fig 34.

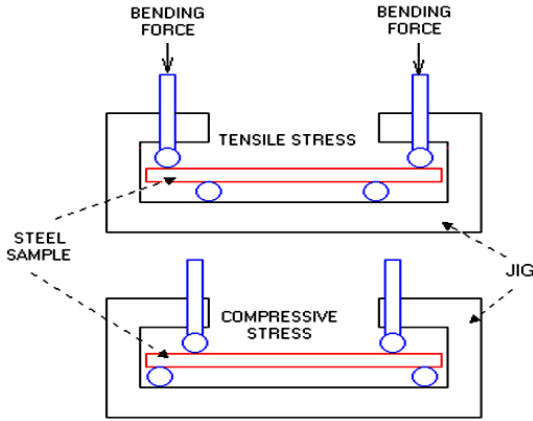


Fig. 33. Four point bending of steel samples to introduce the desired bulk stress state on the sample surface [17]

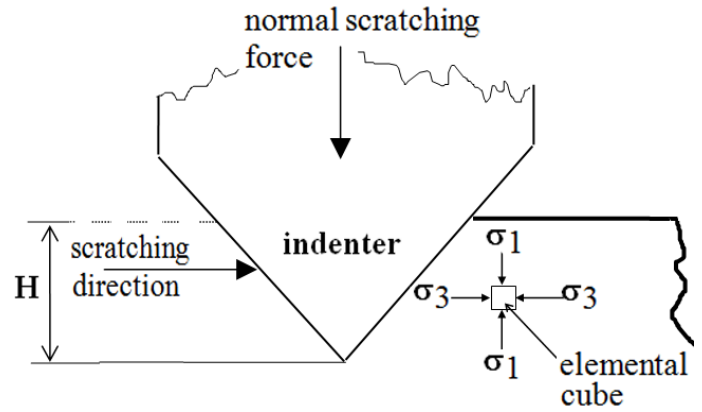


Fig. 34. Stress system during the scratching in the presence of bulk stress [17, 26]

Denote by  $\sigma_1$  = stress collinear with the direction of normal scratching force,  $\sigma_2$  = stress in the direction perpendicular to both normal force vector and to the longitudinal axis of the scratch groove, and  $\sigma_3$  = stress collinear with the scratching direction (i.e. perpendicular to both  $\sigma_1$  and  $\sigma_2$ ). Assume that only  $\sigma_2$  is significantly affected by bulk stress, therefore in the presence of compressive stress it holds  $\sigma_{2compress} < 0$ , while for bulk tension  $\sigma_{2tens} > 0$ . In the case of scratch testing it can be assumed that  $\sigma_1 < 0$  and  $\sigma_3 < 0$ .

According to von Mises' criterion, yielding starts when the second invariant of the stress deviator exceeds some critical value, i.e. if the following inequality is satisfied:

$$\sqrt{0.5((\sigma_1 - \sigma_2)^2 + (\sigma_2 - \sigma_3)^2 + (\sigma_3 - \sigma_1)^2)} > k\sqrt{3}.$$

If  $|\sigma_{2tens}| = |\sigma_{2compress}|$ , then

$$(\sigma_1 - \sigma_{2tens})^2 > (\sigma_1 - \sigma_{2compress})^2$$

and

$$(\sigma_{2tens} - \sigma_3)^2 > (\sigma_{2compress} - \sigma_3)^2,$$

and therefore it holds:

$$\begin{aligned} & \sqrt{0.5((\sigma_1 - \sigma_{2tens})^2 + (\sigma_{2tens} - \sigma_3)^2 + (\sigma_3 - \sigma_1)^2)} > \\ & > \sqrt{0.5((\sigma_1 - \sigma_{2compress})^2 + (\sigma_{2compress} - \sigma_3)^2 + (\sigma_3 - \sigma_1)^2)}. \end{aligned}$$

From the above analysis it follows that in the presence of bulk tension, the conditions for plastic deformation are reached more readily than in the presence of bulk compression. Yielding

process then follows with accompanying effects of the shearing and eventually cutting of material. Therefore, a groove produced by scratch abrasion will be deeper in the presence of tension than compression, Fig 35.

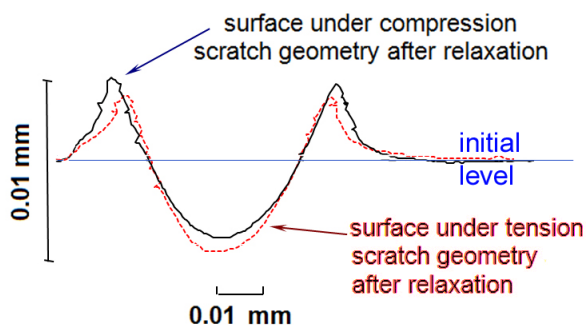


Fig. 35. Diagram of the scratch geometry measured by Taylor-Hobson Talysurf [17, 26]

The scratch groove depth is measured relative to the initial level of unscratched surface. The plastic waves along the scratch sides reach higher upwards under the 12 Spear heating torch Spear tip nails compression compared to tension, while the groove depth is larger in tension than in compression states. Although this inference is supported by statistics [26], a more complete understanding of the reaction of the surface on abrasion can be gained only by means of metallography, Figures 31, 32 and 36.

During an actual hot rolling process, the tool surface is also exposed to mechanical and thermal shocks at the instant of the work piece entry in the deformation zone. One of the authors of this paper (Spuzic) observed over the years of industrial practice the irregularly distributed stains (patches) on the surface of newly re-dressed roll. After re-dressing the roll surface was geometricaly free of indentations in the region of these stains, however, it was apparent that the subsurface microstructure was different compared to the surrounding area. One logical explanation is that this was caused by occasional impacts. When the front edge of the rolled bar is incidentally held for too long under the stream of the roll cooling water its edges can become quenched. This type of accidents is likely to take place at the initial passes, if the draft is high and the rolling velocity significant. Heavy feed such as continuously cast slabs can easily deflect from the rolling line, and then the bar with quenched edges (covered with hard oxides) bounces back instead of being pulled into the deformation zone. Figures 14 and 37 illustrate this scenario. The probability of thermo mechanical shocks increases significantly during the subsequent attempts to roll such bars.

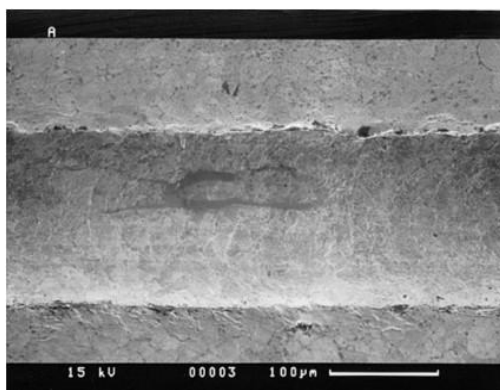


Fig. 36. SEM micrograph of a single scratch made on a polished surface of adamite “A” sample; plastic deformation slip lines can be observed within the scratch bead [17]



Fig. 37. Hot steel slab with quenched edges [27]

Bruises on the surface of the rolls are likely to pick up the scale and some of the hot steel during one rotation and imprint this contamination back to the rolled surface during the following turns. None of the above testing methods enables simulation of this kind of roll surface deteriora-

tion. In particular, laboratory tests seldom reproduce thermal fatigue, as well as thermal and mechanical shocks all of which is frequently observed during the actual hot rolling process [9].

Therefore the authors devised a pilot testing configuration to enable reproducing such hot impacts on the roll materials surface. This inexpensive «hot impact test» consists of a small plain carbon steel spear held in a tube above the sample surface. The design allows for heating the tip of the impact spear to very high temperatures above 1000°C by a flame torch, Figure 38.

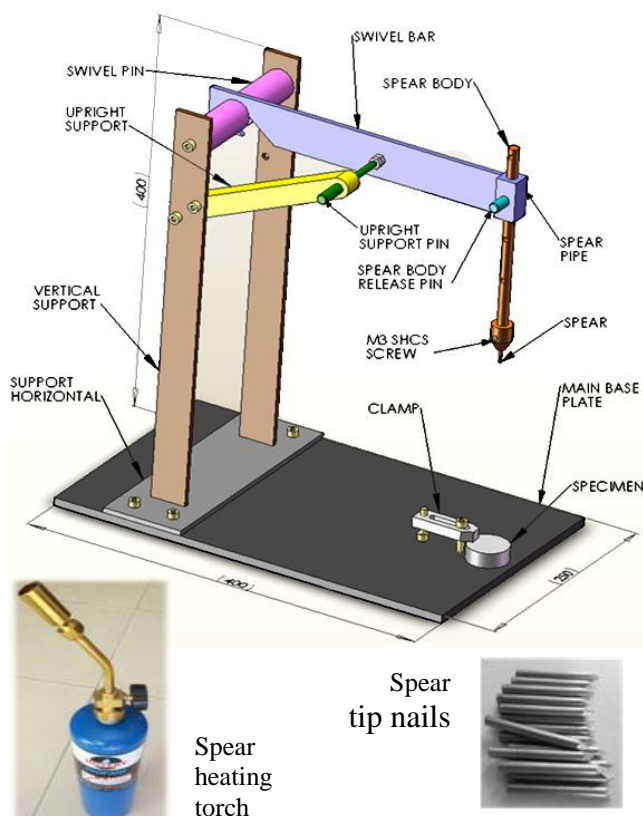


Fig. 38. Hot impact test configuration [28]

In the pilot experiments the low carbon steel spear tip and its base are heated to above 800°C. Then, immediately before the spear is released, the surface of the specimen is wetted by water. When the spear is released, its free fall will create an impact at a very limited area, hence the stress will be significant. The impact must produce only a local surface damage, a shallow limited area ("crater") on the surface where the surface topography and microstructure are to be changed due to the impact contact with the hot pin tip. Several impact forces were used in the range between 100 and 300 N.

It is hypothesised that the nature of the surface damage and the topography change depend on the sample material, impact force magnitude and angle relative to the sample surface. Sample must be thick enough to prevent the cross-section fracture, and also to eliminate the influence of the side faces and edges on the surface to be exposed to the impact. The way of clamping the sample in the holder must ensure that there are only the controlled or no stresses present on the surface to be exposed to hot impact.

Pilot tests are conducted on roll material samples made out of graphitic cast steel of chemical and mechanical attributes shown in the Table below, and microstructure before exposure to hot impact shown in Fig 39.

Figures 40 to 42 show the impact affected zone for this graphitic cast steel. The microstructure does not reveal microcracks at a level above 5-10 micrometers. Only at a very high magnification, at a level below 1 micrometer shown in Figure 42, the crack nucleation can be suspected at the level on nanometers.

Chemical element %	C	2.08
	Si	0.997
	Mn	0.796
	Cr	1.36
	Ni	2.79
	Mo	0.662
	Mg	0.04
	P	0.026
	S	0.025
Hardness Shore		52 – 56
Hardness Rockwell C		40 – 43
Tensile strength, MPa		550 – 800
Bending strength, MPa		900 – 1200

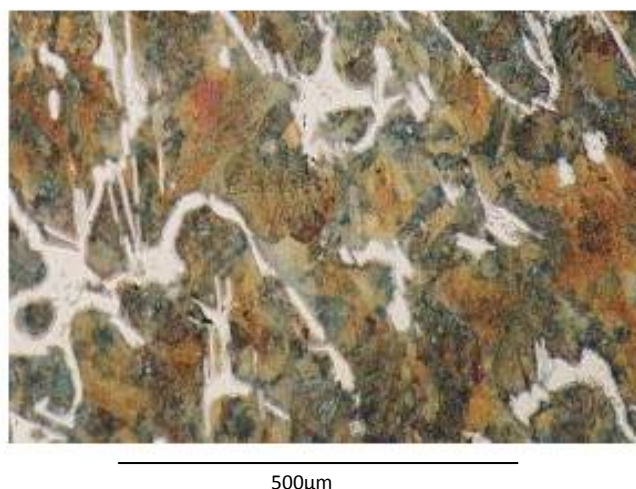


Fig. 39. Pearlitic matrix with dispersed secondary carbides. This is a high-carbon (hypereutectoid) steel, normalised and stress relieved. This material is designed to combine high strength with good wear resistance against fire cracking [23]

When the undamaged surface of the same material was slightly inclined and exposed to another impact at a higher force, the affected region was found to be covered by the remnants of the mild steel and oxides from the hot spear tip, Fig 43.

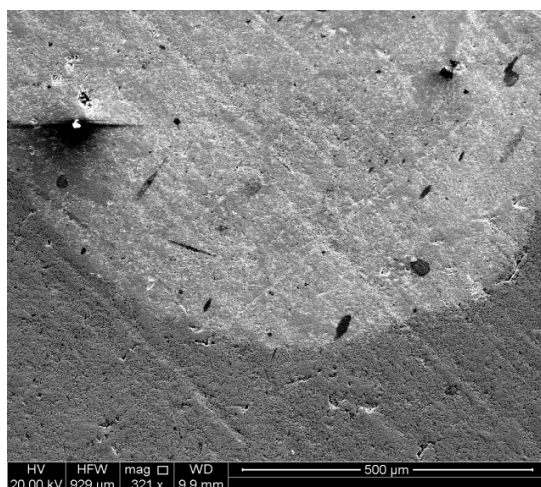


Fig. 40. Unetched topography after exposure to hot impact (graphitic cast steel)

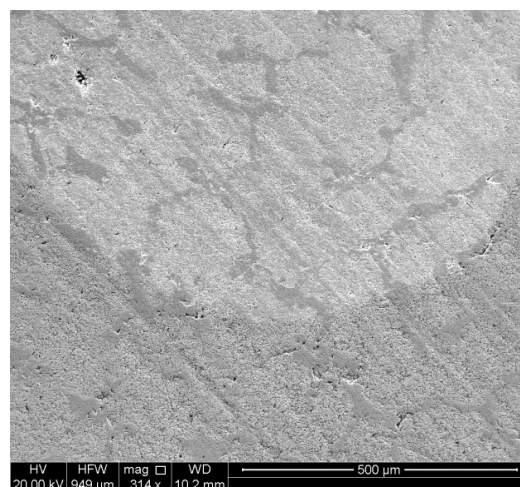


Fig. 41. Impact affected region presented in Fig 39, however, now after light etching with 2.5% Nital. It appears that the microstructure resisted well to thermo-dynamical shock

Observations shown in Figures 43-47 indicate that some materials from the hot spear tip has adhered to the roll surface. This was confirmed by EDX analysis.

Yet another series of observation (Fig 48-53) was made after a third impact was performed on undamaged surface of the same sample. The impact force was significantly lower compared to the previous two cases.

EDX analysis has indicated the presence of oxygen within the impact zone, which further implies the adherence of the oxides from the indenter tip. Such local patches of adhered mixture of hot steel and its oxides are likely to be imprinted back on the incoming rolled surface. Such stains can be further imprinted during the following passes, and all this affects adversely the surface quality of the final product. In any case, the roughness of the impact affected zone is changed relative to the surrounding area of the roll surface (Figures 50 and 51).

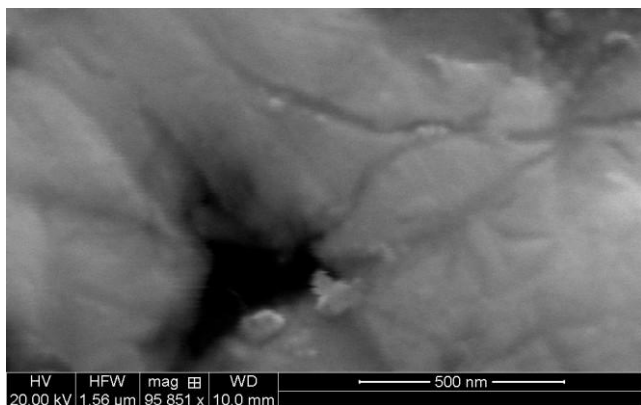


Fig. 42. A local magnification of impact affected zone showing possible crack nucleation

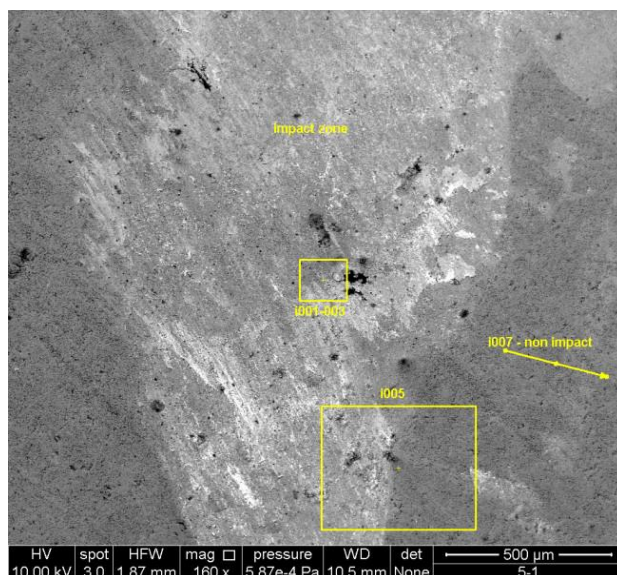


Fig. 43. Unetched topography after an impact at a slight angle and a higher force

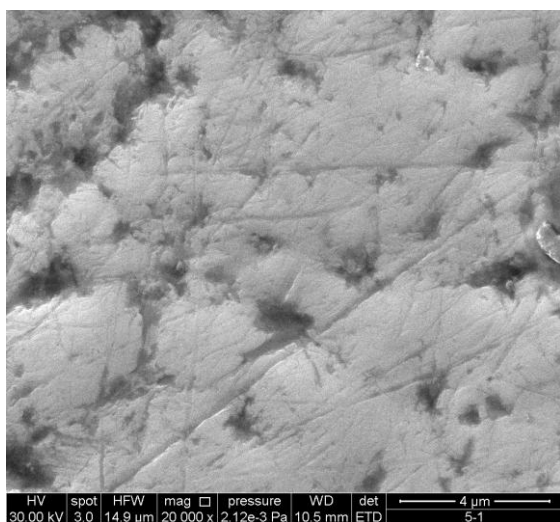


Fig. 44. High magnification of unetched surface outside the impact zone (at the tip of the arrow shown in Fig 43)

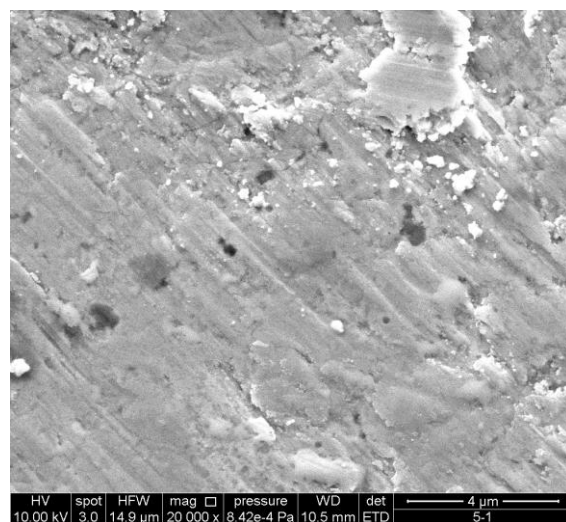


Fig. 45. High magnification of unetched surface within the impact affected area (shown within the smaller square in Fig 43)

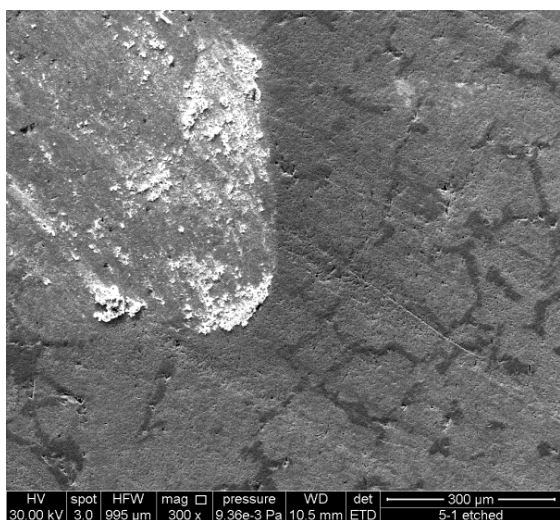


Fig. 46. Topography of the region within the larger square shown in Fig 43. Sample surface is etched after the impact with 2% Nital

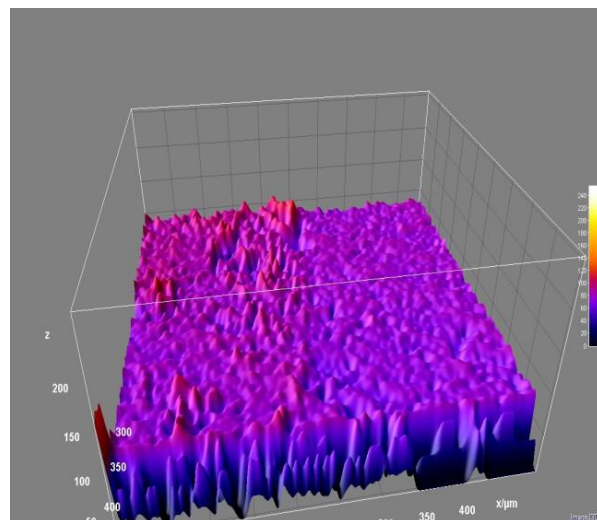


Fig. 47. 3D image processing of the topography shown in SEM micrograph in Fig 46

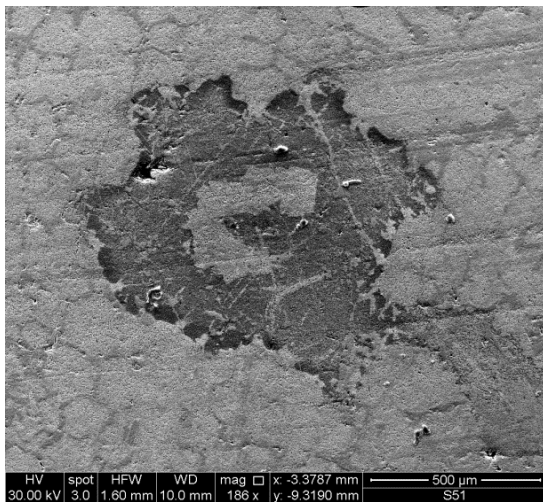


Fig. 48. SEM micrograph (secondary electron scan) of the impact area (etched with 2% Nital)

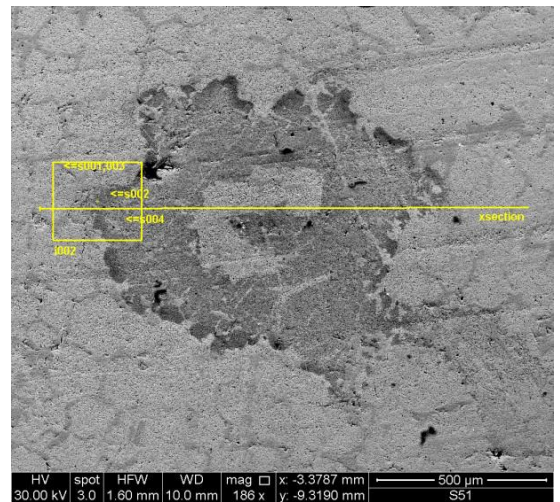


Fig. 49. Mixed SEM image based on mixture of backscattered electrons and secondary electrons scans

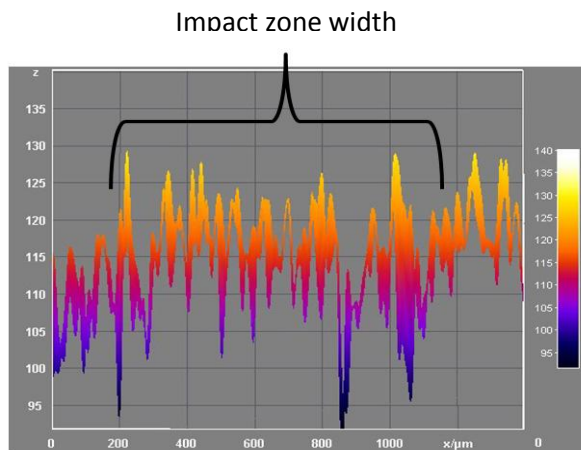


Fig. 50. Surface topography profile along the line shown in Fig 49. Note the plastic waves near the impact zone boundaries. (Horizontal axis is real; vertical axis is distorted while still maintaining relative vertical distance ratios)

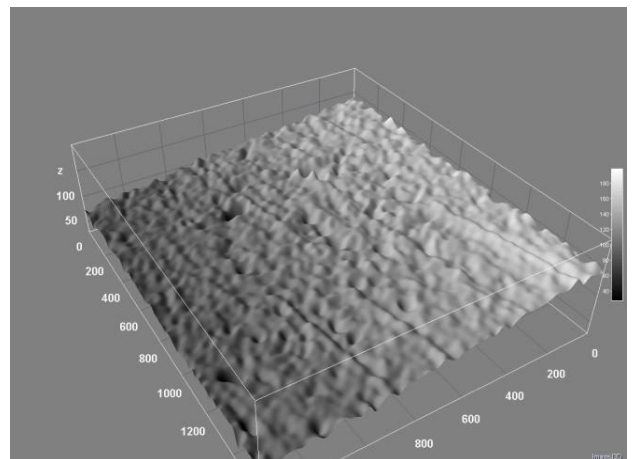


Fig. 51. 3D image processing of the topography shown in SEM micrograph in Fig 49 (Horizontal axis is real; vertical axis is distorted while still maintaining relative vertical distance ratios)

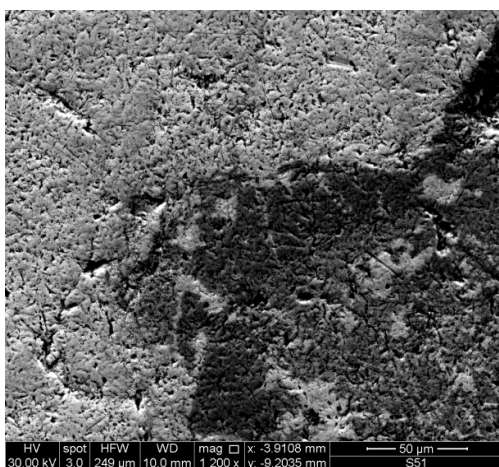


Fig. 52. SEM micrograph (secondary electron scan) of the area within the square marked in Fig 49

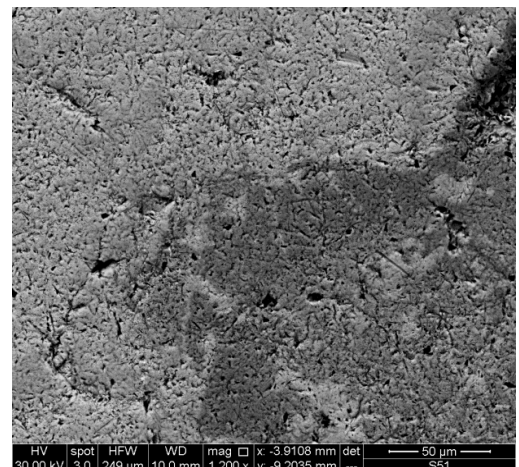


Fig. 53. SEM micrograph based on mixture of backscattered electrons and secondary electrons scans. The area within the square marked in Fig 49

Another type of the roll material – an alloyed cast iron with nodular graphite embedded in pearlitic matrix with carbide spots – was exposed to similar pilot test using the above hot impact configuration. The attributes for this grade, considered to be suitable for hot rolling in roughing and intermediate stands, are shown in Table below. Microstructure of material before exploitation is shown in Fig 54.

C (%)	Si (%)	Mn (%)	Cr (%)	Ni (%)	Mo (%)
3.28	1.32	0.63	0.57	1.65	0.14
Barrels Hardness HRC		Tensile Strength (N/mm <sup>2</sup> )		Bending Strength (N/mm <sup>2</sup> )	
34 - 37		450-700		700 -1100	



150 μm

Fig. 54. Pearlitic matrix with carbides and nodular (spheroidal) graphite

The figures below show the results of a mild impact with a hot steel pin. Impact is conducted at the angle 90° (perpendicular) to the sample surface.

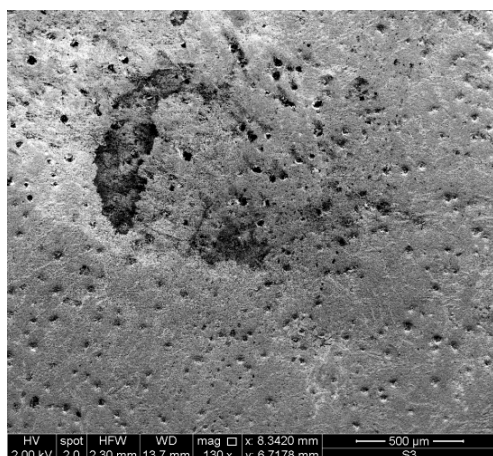
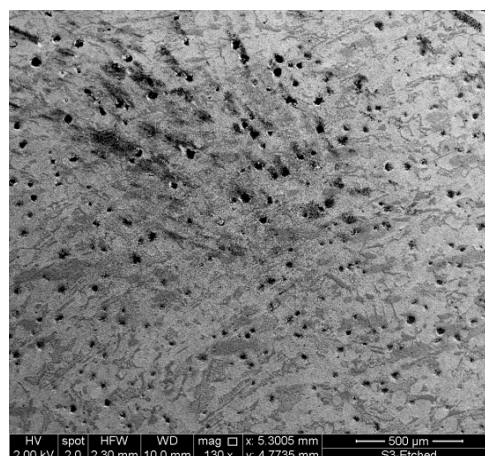


Fig. 55. SEM micrographs of unetched surface showing the impact zone (based on mixture of backscattered electrons and secondary electrons scans)



The same impact zone (surrounded by the impact-unaffected area) after etching with 2% Nital. A plastic distortion can be observed especially in the graphite nodule boundaries

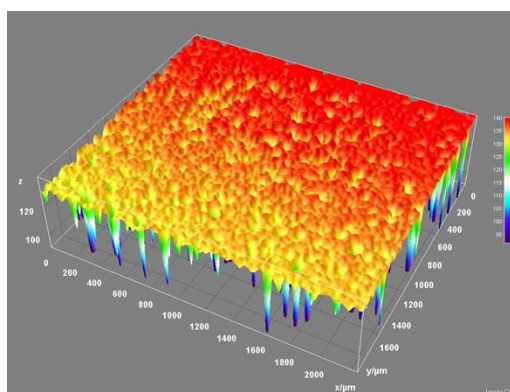


Fig. 56. 3D image analysis presenting the impact zone topography of the area shown in Figures 54 and 55 (horizontal axis is real, vertical axis is distorted while still maintaining relative vertical distance ratio)

In the case of this roll materials, which is softer in comparison to the graphitic cast steel shown in Figures 39 to 53, the plastic deformation is visible especially along the impact zone boundaries and around the graphite nodule perimeters.

### 3. DISCUSSION AND CONCLUSIONS

Design tasks in rolling technology today can be performed with the help of advanced data processing tools. The growing industrial and other published data base is increasingly available for systematic exploration of patterns that can be correlated to the performance of actualised processes.

The comprehensive numerical data defining the product and process attributes can be organised within structured matrices and analysed using powerful information processing platforms. However, this strategy must be realised without triggering unnecessarily complex mathematical structures.

Geometric and dynamic entries can be organised to introduce higher uniformity in the definition of the deformation zone in rolling as shown in section 2.2.

Notwithstanding the usefulness of the trends prompting for continuous improvements and new developments in product quality, the product attributes are usually well standardised. However, at the instant of introducing new products, and in some instances of existing products, certain specifications can be negotiated to relax too stringent requirements on the manufacturers. These issues too can be anticipated or diagnosed most efficiently by systematic reviewing the industrial data bases.

On the other hand, both the roll pass design and the tool materials are intrinsically prone to become overcome or even obsolete from the point of view of costs, efficiency and resource consumption or otherwise overall sustainability.

Selection of tool materials is greatly affected by the conventions used in defining the material attributes. In addition, the hierarchy and significance of these attributes depend on the type of the rolling mill and the stage (break-down, intermediate or finishing) of the process. Roll manufacturers often address this aspect of the groove geometry, when offering various roll materials, e.g. by suggesting that a particular grade is suitable for “rolls with deep grooves”. In this regard the methods presented in section 2.3 would greatly advance if the relevant research continues by means of more detailed experimenting scrutiny. Hot impact test is an inexpensive method that can be used to compare reaction of differing roll grades to hot impact at differing angles. High resolution (SEM and TEM) materialography examination will reveal the increase in the microcrack density within the impact zone compared to the impact-unaffected zone. The character of the deformed zone can be evaluated with regard to the brittleness and fire crack resistance. Finally, the propensity to the debris (oxide scale and hot steel residues) adherence can be evaluated in line with the roughness changes.

In addition to systematically analysing the records from realised manufacturing processes roll pass designers have to their disposition data bases collected by virtue of a whole spectrum of laboratory simulation and testing methods. It is of great interest to develop more accurate methods to assess the roll performances and criteria for their selection as well [18].

Moreover, numerous researchers continue to experiment with novel approaches. The contemporary communication systems make it possible to exchange advancing knowledge at the unprecedented rates. Transparent sharing of results is the most efficient way of validating the explored hypotheses. The nucleation of new ideas is enhanced by encouraging cross disciplinary insights. For example, the experiments with chamfered front end open the way for exploring potentials for achieving a range of benefits such as:

- An increase in roll bite at the initial passes can in some instances eliminate two passes at the rougher break-down mill rolling schedule;
- Due to increased drafts at the initial passes, the reduction at the following passes can be decreased thus enabling better dimensional control;
- New technique lowers the probability of the interfacial damage at the rougher rolls and also downstream the rolling process;

- Duration of the rolling will decrease (even if two passes are not eliminated, because the rolling speed can be increased);

- Roll consumption will decrease and the quality of the product will increase.

The idea of introducing generic matrices to define the deformation process in rolling opens the doors for extracting useful knowledge from industrial and otherwise published databases. This has ultimate potentials to help generating design solutions resulting with benefits such as:

- The energy and other resource (water, tool) consumption will decrease;

- Overall plant productivity, yield and reliability will increase;

- Production costs will decrease while improving the control of the product quality.

All above effects ultimately lead to a contribution to a more sustainable rolling process.

The presented strategies, techniques and inferences need to be subject to further research scrutiny in order to provide further evidence, however, the discussed ideas and pilot results uncover new avenues where the progress in optimising the rolling mill technology can be sought for. Precondition for these advances is in overcoming the formal barriers in communicating knowledge between industry and academe.

## REFERENCES

1. M.Ellis, S.Dillich, N.Margolis, report “Industrial Water Use and Its Energy Implications”, Energetics Incorporated and U.S. Department of Energy–Office of Industrial Technologies, 2011, p. 4.
2. J.Hill et al: report titled “Water Proofing Adelaide - A thirst for change 2005 – 2025”, Government of South Australia, Crown in right of South Australia, 2005.
3. V.Oduguwa and R.Roy: International Journal of Machine Tools and Manufacture, 2006, vol 46(7-8), pp. 912-928.
4. H.J.McQueen and W.J.McGregor Tegar: Sci. Am., 1975, 232 (4), pp 116-125.
5. S-E.Lundberg, S-E.: Scandinavian Journal of Metallurgy, 1997, vol. 26 (3), pp.102-114.
6. E.Appleton and E.Summad: “Roll pass design: a ‘design for manufacture’ view”, 2nd European Rolling Conference at AROS Congress Center, Västerås, Sweden May 24 - 26, 2000.
7. F.E.Dolzhenkov : Metallurgical and Mining Industry 2009, No 1, pp. 33-37.
8. K.Abhary, K.Garner, Z.Kovacic, S.Spuzic, F.Uzunovic and K.Xing: Key Engineering Materials, 2010, vol. 443, pp. 3-8.
9. M.Pellizzari, D.Cescato, M.G.De Flora: Wear, 2009, vol. 267(1–4), pp. 467-475.
10. Anon.: “Roll Failures Manual - Hot Mill Cast Work Rolls”, 1st ed., 2002, The European Foundry Association CAEF.
11. Anon.: product catalogue, The Akers Group, viewed on 1September 2013 at <http://www.akersrolls.com>
12. Anon.: product catalogue, Union Electric Steel, viewed on 1st September 2013 at <http://uniones.com>
13. Anon.: product catalogue, Gontermann-Peipers viewed on 1st September 2013 at GmbH <http://www.gontermann-peipers.de>
14. Anon.: product catalogue, Eisenwerk Sulzau-Werfen, viewed on 1st September 2013 at <http://www.esw.co.at>
15. Anon.: product catalogue, Marichal Ketin, viewed on 1st September 2013 at <http://www.mkb.be/>
16. Anon.: product catalogue, Innse Cilindri s.r.l., viewed on 1st September 2013 at <http://www.innsecilindri.com>
17. S.Spuzic, Hot Rolling Mill Roll Wear - Some Aspects of High Temperature Abrasion, Ph.D Thesis, The University of South Australia, Adelaide, 1996.
18. M.Pellizzari, A.Molinari, G.Straffelini: Wear, 2005, vol. 259(7–12), pp. 1281-1289.
19. S.Spuzic, M.Zec, K.Abhary, R.Ghomashchi, I.Reid: Wear, 1997, vol. 212 (1), pp. 131-139.
20. N.F.Garza-Montes-de-Oca, W.M.Rainforth: Wear, 2009, vol. 267(1–4), pp. 441-448.

21. J.Vojkovský, J.Veščík, and A.Velsovský: Roll Pass Designer's Handbook for a Section Rolling Mill (in Czech: Příručka kalibréra ve válcovně profilů), Nakladatelství technické literatury, Praha, 1968, pp. 102-104.
22. S.Spuzic, K.Abhary, invited lecture "A Contribution to Rolling Mill Technology - Roll Pass Design Strategy for Symmetrical Sections", 83rd AIKW (Association of International Roll Pass Designers and Rolling Mill Engineers) conference, 9th to 11th October 2013, Ostrava / Czech Republic <http://www.aikw.org>
23. Anon.: product catalogue, Chodan Sazan, viewed on 1st September 2013 at <http://www.csroll.com>
24. U.Stahlberg and A.Goransson: Journal of Mechanical Working Technology, 1986, 12, pp. 373-384.
25. S.Spuzic, K.N.Strafford, C.Subramanian, G.Savage: Wear, 1994, vol. 176, pp. 261-271.
26. S.Spuzic, K.N.Strafford, C.Subramanian, L. Green: Wear, 1995, vol. 184, pp. 83-86.
27. Anon.: Steel photo gallery, a steel industry news and information portal, Steelonthenet.com viewed on 1st September 2013 at [www.steelonthenet.com](http://www.steelonthenet.com)
28. Panduranga Hubli, Hot Rolling Mill Roll Wear Hot Impact, Final Year Project report submitted for the degree of Bachelor of technology in Mechanical and Manufacturing engineering, School of Engineering, University of South Australia, 2013.
29. V.K.Smironov, V.A.Shilov, Y.V.Inatovich: Roll Pass Design for Rolling Mill Rolls, Metallurgija, Moscow, 1987, p. 266.

М.И. Румянцев, Д.Н. Чикишев, И.А. Разгулин  
ФГБОУ ВО «Магнитогорский государственный  
технический университет им. Г.И. Носова»

## ОПЫТ КОНСТРУИРОВАНИЯ МОДЕЛИ ДЛЯ РАСЧЕТА МОМЕНТА ПРОКАТКИ НА ТОЛСТОЛИСТОВОМ СТАНЕ

Выполнен анализ погрешности прогноза момента при прокате толстых листов в зависимости от известных методик расчета коэффициента плеча.

Ключевые слова: прокатка толстых листов, момент прокатки, высота очага деформации, коэффициент плеча, высотная утяжка.

При совершенствовании технологических систем листовой прокатки большое значение имеет задача определения момента прокатки, который в соответствии с известным подходом выражается через усилие прокатки  $P$  с использованием коэффициента плеча  $\psi$ :  $M = 2P\psi l_x$  (здесь  $l_x$  – длина геометрического очага деформации). Для вычисления  $\psi$  существует множество различных формул. Однако они были получены при различных условиях прокатки и применение каждой из них в иных условиях будет приводить к заметным погрешностям оценки момента прокатки. Поэтому в работе была поставлена задача выбора формул, которые дают наименьшую погрешность в конкретных условиях прокатки.

В качестве экспериментальных данных использовали результаты наблюдений при прокатке на стане 5000 раскатов толщиной 12,0-25,4 мм и шириной 2620-4500 мм из сталей марок Ст3сп, 15ХСНДА, категорий прочности К65 (2 паспорта) и Х65, которые также анализировались в предыдущей работе [1]. Настоящий эксперимент включал 87 опытов, каждый из которых соответствовал прокатке одного из листов. Усилие прокатки изменялось в диапазоне 20-97 МН (рис. 1), а момент прокатки – от 1000 до 8000 кНм (рис. 2). В качестве определяющего фактора приняли характеристику высоты очага деформации  $l_x/h_{cp}$ , расчетные значения которой оказались в пределах от 0,64 до 2,88.

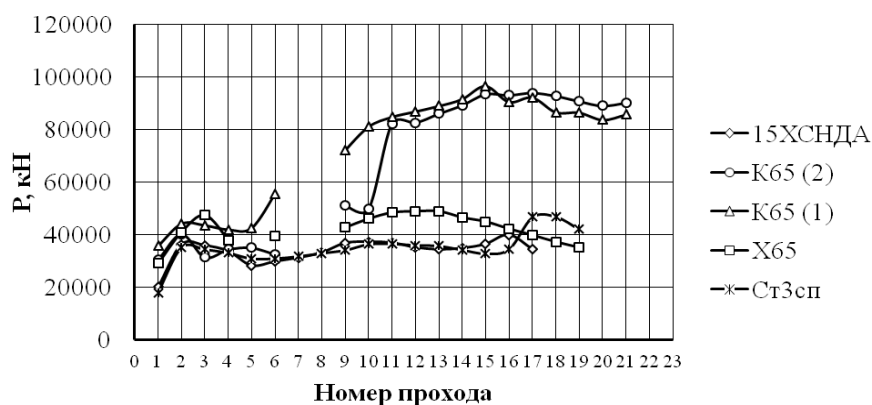


Рис. 1. Усилие прокатки для различных марок сталей по проходам

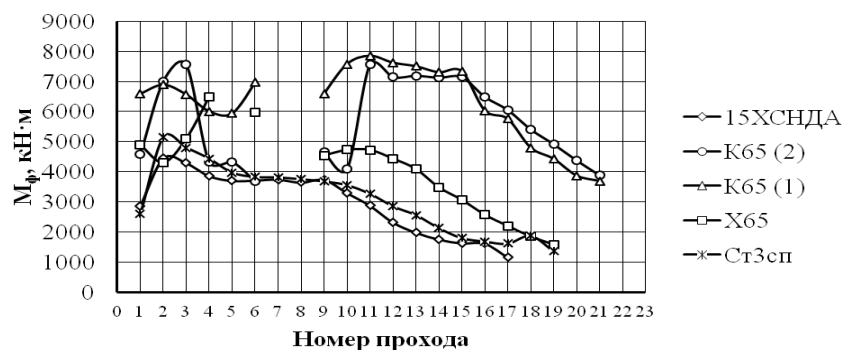


Рис. 2. Момент прокатки для различных марок сталей по проходам

Фактические значения коэффициента плеча рассчитывали по известной формуле:

$$\psi_{\Phi} = \frac{M_{\Phi}}{2Pl'_x}, \quad (1)$$

где  $l'_x$  – длина очага деформации с учетом высотной утяжки [2]:

$$l'_x = l_x \sqrt{1 - \nu_h}; \quad (2)$$

$\nu_h$  – степень высотной утяжки:

$$\nu_h = 0,115 \left( \frac{l_x}{h_{cp}} \right)^{-0,7}. \quad (3)$$

Расчетные значения  $\psi$  определяли по формулам, авторами которых являются: З.Вусатовский [3, (I.290)]; М.М.Сафьян, В.И.Мелешко [3, с.95]; Д.Н.Калинский [3, с.95]; Ю.В.Полторапавло, П.П.Поляков и др. [3, с.95]; М.И.Бояршинов, В.П.Полушкин [3, с.95]; В.М.Луговской [3, с.95]; В.С.Смирнов, А.К.Григорьев и др. [3, с.95]; Э.А.Орнатский, В.М.Клименко и др. [3, с.96]; Д.И.Суяров, Ф.С.Гилевич [3, с.95].

Сравнив относительные погрешности расчета коэффициента плеча по указанным формулам с результатами расчетов по формуле (1) установили, что при  $l'_x/h_{cp} < 1,4$  наименьшая погрешность наблюдается при использовании формулы Д.И.Суярова и Ф.С.Гилевича:

$$\psi = 0,4915 + 0,518 \frac{l'_x}{h_{cp}} - 0,7068 \left( \frac{l'_x}{h_{cp}} \right)^2 + 0,258 \left( \frac{l'_x}{h_{cp}} \right)^3 - 0,02 \left( \frac{l'_x}{h_{cp}} \right)^4. \quad (4)$$

В диапазоне  $1,4 \leq l'_x/h_{cp} < 2$  предпочтительно использовать формулу З.Вусатовского:

$$\psi = \frac{h_1}{2\Delta h} \ln \frac{h_0}{h_1}. \quad (5)$$

Для случаев прокатки когда  $l'_x/h_{cp} \geq 2$ , рекомендуем применять формулу М.М.Сафьяна и В.И.Мелешко:

$$\psi = 0,498 - 0,0283 \frac{l'_x}{h_{cp}}. \quad (6)$$

Алгоритм расчета коэффициента плеча, учитывающего указанные особенности, приведен на рис. 3.

Степень соответствия между коэффициентом плеча, рассчитанным по данному алгоритму и фактическим значением  $\psi_{\Phi}$  составляет 82% (рис.4), а расхождение прогнозируемого и фактического момента прокатки не превышает 1% (рис. 5).

Для оценки важности и обоснования необходимости учета высотной утяжки в исследованиях процесса толстолистовой прокатки выполнили подобные расчеты, целенаправленно не рассматривая данное явление. В этом случае степень соответствия прогнозируемых и фактических значений  $\psi$  уменьшается до 59% (рис. 6). Вместе с тем степень соответствия прогнозируемых и фактических значений момента прокатки остается достаточно высокой – 98% (рис.7).

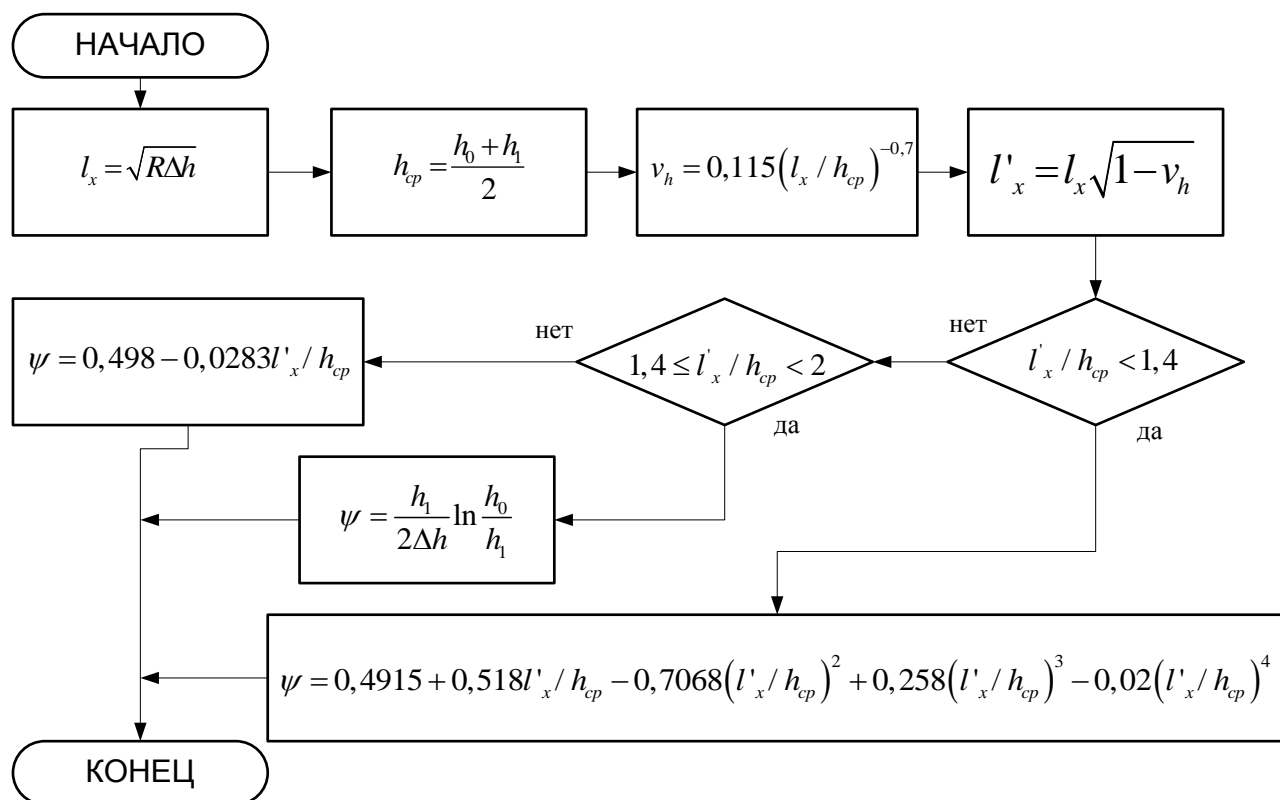


Рис. 3. Алгоритм расчета коэффициента плеча

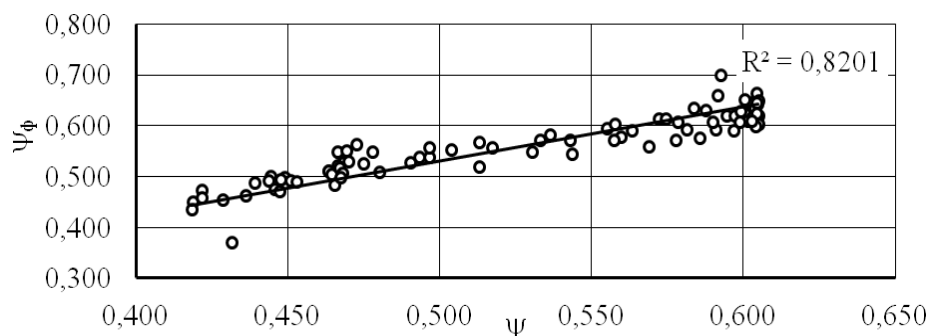


Рис. 4. Диаграмма соответствия фактических и рассчитанных значений коэффициента плеча с учетом высотной утяжки

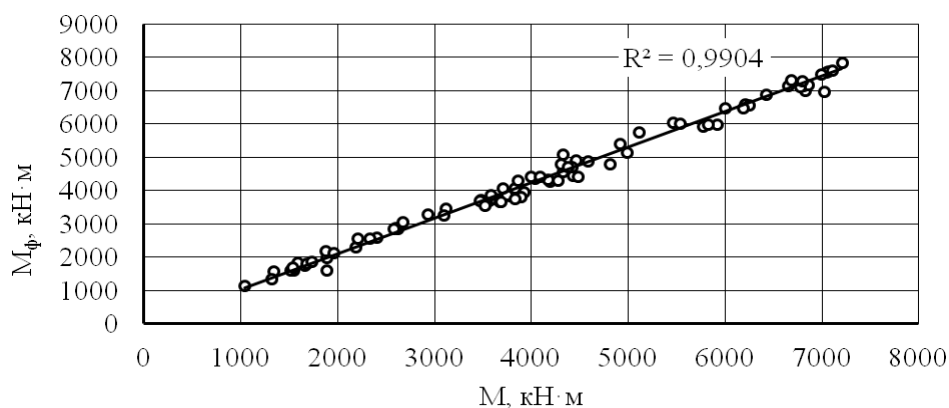


Рис. 5. Диаграмма соответствия фактических и рассчитанных значений момента прокатки с учетом высотной утяжки

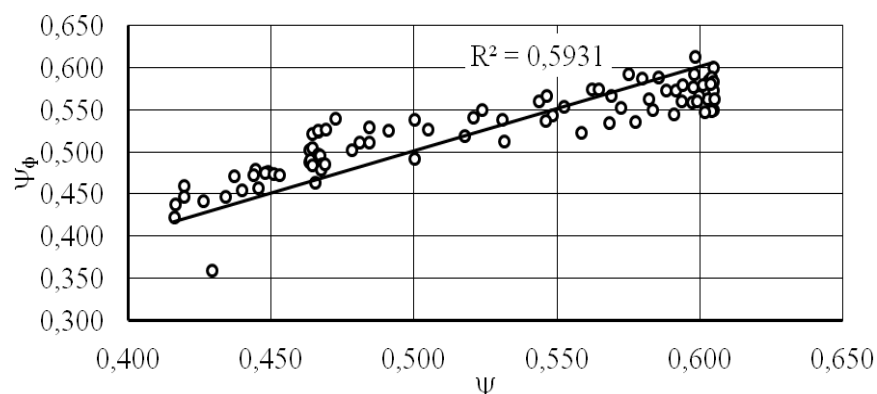


Рис. 6. Диаграмма соответствия фактических и рассчитанных значений коэффициента плеча без учета высотной утяжки

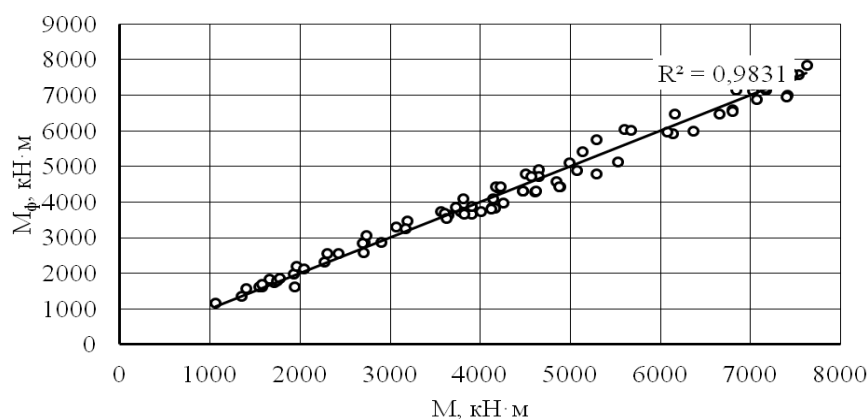


Рис. 7. Диаграмма соответствия фактических и рассчитанных значений момента прокатки без учета высотной утяжки

Таким образом разработан алгоритм расчета момента прокатки толстых листов, который позволяет обеспечить высокую точность прогноза за счет выбора формул для определения коэффициента плеча в зависимости от характеристики высоты очага деформации  $l_x/h_{cp}$ . Если учитывать высотную утяжку полосы на входе металла в валки, что особенно важно при  $l_x/h_{cp} < 1$ , степень соответствия прогнозируемых и фактических значений коэффициента плеча достигает 82%. Если высотной утяжкой пренебречь, степень соответствия рассчитанного и фактического  $\psi$  уменьшается до 59%. В обоих случаях степень соответствия моментов прокатки составила 98-99%.

#### Библиографический список

1. Румянцев М.И., В.И. Белов, И.А. Разгулин. Опыт совершенствования методики Л.В.Андреюка для расчета напряжения текучести при горячей листовой прокатке. Электронный журнал «Калибровочное бюро» 5 выпуск, с.73–84, 2015г. URL: [http://passdesign.ru/numbers/number\\_five\\_05\\_2015.zip](http://passdesign.ru/numbers/number_five_05_2015.zip) (дата обращения: 10.02.2016).
2. Грудев А.П. Теория прокатки. Изд-е 2-е, перераб и доп. М.: Интермет Инжиниринг. 2001. 280с.
3. Коновалов Ю.В., Остапенко А.Л., Пономарев В.И. Расчет параметров листовой прокатки. Справочник. М.: Metallurgia, 1986.

М.И. Румянцев, Д.Н. Чикишев, И.А. Разгулин  
ФГБОУ ВО «Магнитогорский государственный  
технический университет им. Г.И. Носова»

## ОПЫТ КОНСТРУИРОВАНИЯ МОДЕЛИ ДЛЯ ПРОГНОЗА ТЕМПЕРАТУРЫ МЕТАЛЛА ПРИ ПРОКАТКЕ НА ТОЛСТОЛИСТОВОМ СТАНЕ

Выполнен анализ точности расчета температуры металла при прокатке на толстолистовом стане при использовании различных сочетаний 38 формул, отображающих деформационный разогрев, охлаждение теплопередачей валкам и охлаждение излучением. На основании результата анализа сконструирована аккомодационная модель для прогноза температуры раската перед каждым проходом при стандартной ошибке оценивания  $9^{\circ}\text{C}$ .

Ключевые слова: толстолистовой стан, температура металла, деформационный разогрев, охлаждение теплопередачей валкам, охлаждение излучением, аккомодационная модель.

При совершенствовании технологических систем производства горячекатаной листовой стали большое значение имеет задача прогноза температуры раската. При прокатке толстых листов наиболее существенными составляющими изменения температуры являются: разогрев металла в результате деформации ( $\Delta t_{\eta}$ ), теплоотдача рабочим валкам ( $\Delta t_{cwr}$ ), теплоотдача излучением ( $\Delta t_r$ ). Известно много формул для расчета каждой из указанных составляющих, однако эти формулы были получены при различных условиях прокатки и применение каждой из них в иных условиях может приводить к заметным погрешностям. Поэтому в работе была поставлена задача выбора формул, которые дают наименьшую погрешность в конкретных условиях прокатки.

В качестве экспериментальных данных использовали результаты наблюдений при прокатке на стане 5000 раскатов толщиной 12,0-25,4 мм и шириной 2620-4500 мм из сталей марок СтЗсп, 15ХСНДА, категорий прочности К65 (2 паспорта) и Х65, которые также анализировались в предыдущей работе [1]. Температура начала прокатки ( $t_{0\phi}$ ) изменялась в диапазоне  $770 \div 1070^{\circ}\text{C}$  (рис. 1), усилие прокатки  $P = 20 \div 97 \text{ МН}$ , степень деформации

$\xi = 7,14 \div 21,3\%$ , отношение времени паузы к толщине раската  $\frac{\tau}{h} = 0,04 \div 0,35 \text{ с/мм}$ , от-

ношение длины к средней высоте очага деформации  $\frac{l_x}{h_{cp}} = 0,64 \div 2,88$ , среднее давление

$p_{cp} = 89,17 \div 446,22 \text{ МПа}$ . При выполнении исследования рассматривались только те проходы, в которых не применялись гидросбив окалины и кантовка раската.

Для расчета  $\Delta t_{\eta}$  известны формулы: А.И.Целикова [2, (II.86)]; Л.Г.Стукача [2, (II.87)]; В.А.Тягунова [2, (II.88)]; Н.И.Крендлина [2, (II.90)]; Ю.Д.Железнова, Б.А.Шифриновича [2, (II.91)]; М.А.Зайкова [2, (II.93)]; Х.Венцеля [2, (II.94)]; С.Л.Коцаря, Б.А.Полякова, М.И.Псела [2, (II.95)]; О.Павельски [2, (II.96)]; В.И.Зюзина, М.Я.Бровмана, А.Ф.Мельникова [2, (II.97)]; В.М.Логовского [2, (II.99)]; Ю.В.Коновалова, А.Л.Остапенко, В.И.Пономарева [2, (II.100)].

Расчет  $\Delta t_{cwr}$  может быть выполнен по формулам: В.Тринкса [2, (II.46)]; В.А.Тягунова [2, (II.47)]; Ш.Гелеи [2, (II.49)]; Х.Венцеля [2, (II.52)]; Ю.Д.Железнова, Б.А.Шифриновича [2, (II.54)]; О.Павельски [2, (II.55)]; Ф.Серединского [2, (II.56)]; В.М.Луговского [2, (II.57)]; Ю.В.Коновалова, А.Л.Остапенко [2, (II.58)]; С.Л.Коцаря, Б.А.Полякова, М.И.Псела [2, (II.60)]; И.М.Мееровича, И.Ф.Франценюка, Ю.Д.Железнова и др. [2, (II.61)]; И.Шварцера [2, (II.62)]; В.И.Зюзина, М.Д.Залесова, Л.Д.Ломтева [2, (II.64)].

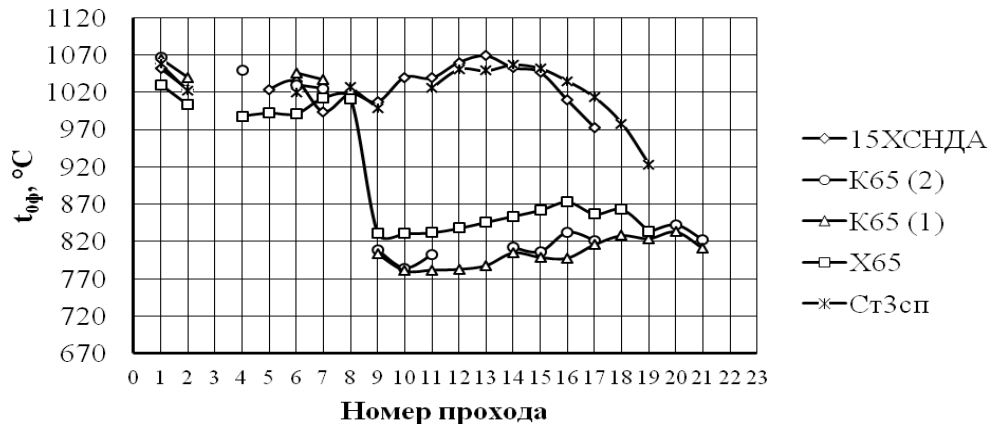


Рис. 1. Температура начала прокатки листов из различных марок стали

Чтобы определить  $\Delta t_r$ , можно применить формулы: В.Тринкса [2, (II.6)]; В.А.Тягунова [2, (II.7), (II.8)]; Г.П.Иванцова [2, (II.9)]; Ш.Гелеи [2, (II.11)]; М.А.Зайкова, В.В.Пудинова [2, (II.13)]; П.В. Ли, Р.Б.Симса, Х.Райта [2, (II.14)]; Н.Н.Крейндлина [2, (II.15)]; Х.Венцеля [2, (II.17)]; А.Ловайя, Г.Кройлича [2, (II.18)]; И.И.Васина, А.Ш.Гиндина [2, (II.19)]; М.М.Сафьяна [2, (II.21)]; И.Шварцера [2, (II.24)]; В.М.Луговского, А.Л.Остапенко [2, (II.26)].

Как и в работах [3-5], для каждого прохода рассматривали различные сочетания  $\{\Delta t_\eta; \Delta t_{cwr}; \Delta t_r\}$  составляя их по принципу перебора всех упомянутых формул. Наилучшим сочетанием для прохода считали такое, при котором различие рассчитанной температуры начала прокатки  $t_0$  и фактической  $t_{0ф}$  было минимальным. Всего было выявлено 27 различных сочетаний, удовлетворяющих требованию  $|t_0 - t_{0ф}| \rightarrow \min$ . Анализ значимости факторов прокатки, которые были выявлены в работах [3-5] показал, что для прокатки на толстолистовом стане наиболее информативным фактором является характеристика высоты очага деформации  $l_x/h_{cp}$ .

Установили, что при выборе формул для расчета изменения температуры листа в результате излучения необходимо рассматривать следующие диапазоны  $l_x/h_{cp}$ : не более 1,87; 1,88÷2,75; 2,76 и более. В указанных диапазонах предпочтительно применять формулы: М.А.Зайкова, В.В.Пудинова; И.Шварцера. Алгоритм расчета представлен на рис 2.

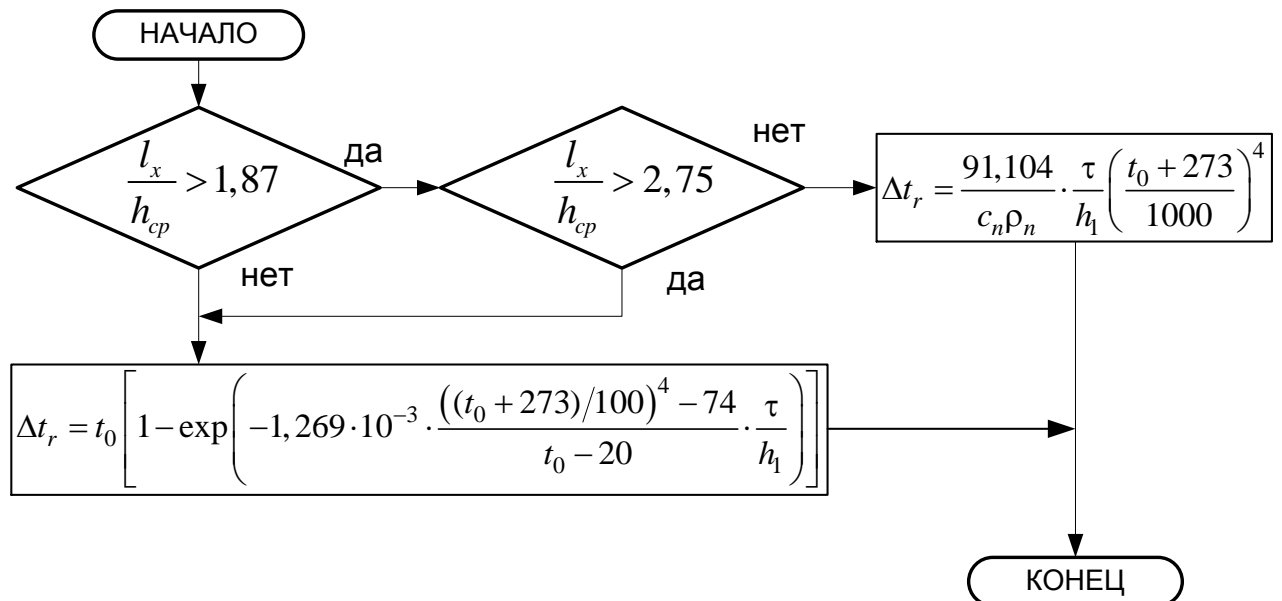


Рис. 2. Алгоритм расчета изменения температуры листа в результате излучения

При выборе формул для расчета изменения температуры листа в результате передачи тепла валкам необходимо рассматривать диапазоны  $l_x/h_{cp}$  до 1,17; 1,17÷1,43; 1,44÷1,48; 1,48÷1,51; 1,52÷1,53; 1,54÷1,87; 1,88÷2,75; 2,76 и более. В указанных диапазонах предпочтительно применять формулы: В.Тринкса; Х.Венцеля; Ю.Д.Железнова, Б.А.Шифриновича. Алгоритм расчета по данной методике представлен на рис 3.

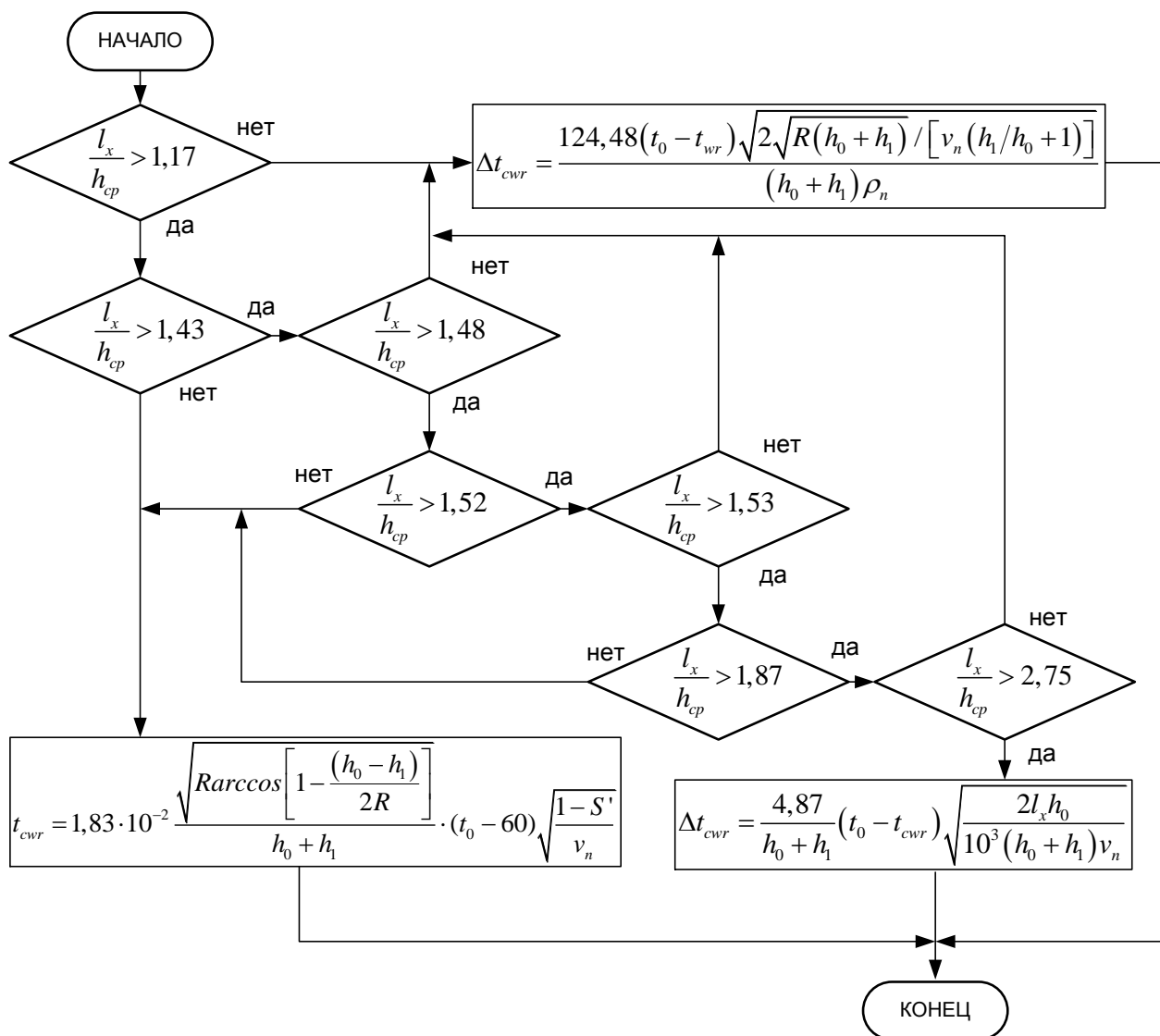


Рис. 3. Алгоритм расчета изменения температуры листа в результате передачи тепла валкам

При выборе формул для расчета изменения температуры листа в результате деформационного разогрева необходимо рассматривать диапазоны  $l_x/h_{cp}$  до 1,17; 1,17÷1,43; 1,44÷1,48; 1,48÷1,51; 1,52÷1,53; 1,54÷1,87; 1,88÷2,75; 2,76 и более. В указанных диапазонах предпочтительно применять формулы: Л.Г.Стукача; В.А.Тягунова; В.И.Зюзина, М.Я.Бровмана, А.Ф.Мельникова. Алгоритм расчета представлен на рис 4.

При использовании разработанных алгоритмов степень соответствия расчетных и фактических изменений температуры между двумя последовательными проходами составила 71% (рис. 5). А степень соответствия между расчетными и фактическими значениями температуры начала прокатки в двух последовательных проходах составила 99% (рис. 6).

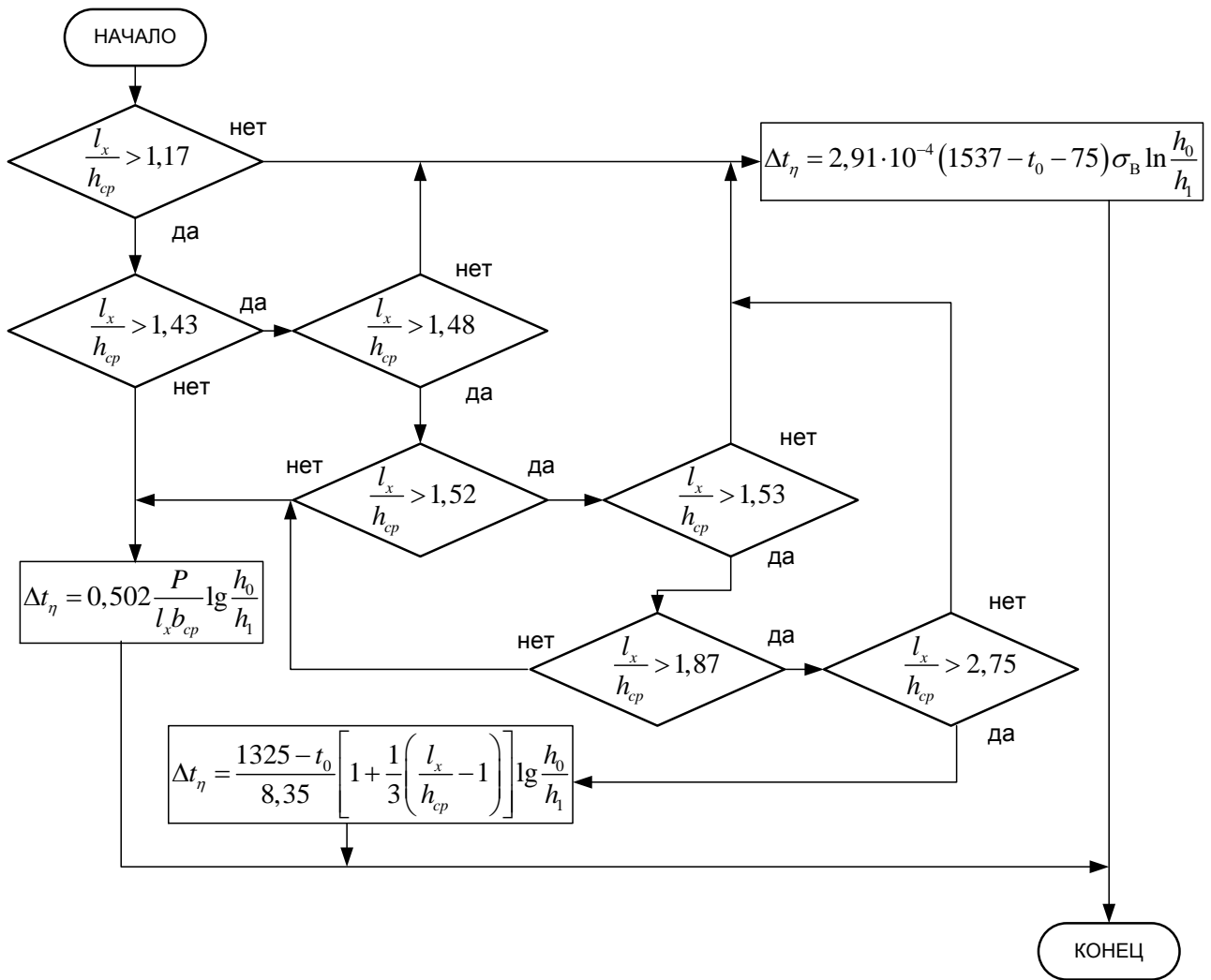


Рис. 4. Алгоритм расчета изменения температуры листа в результате деформационного разогрева

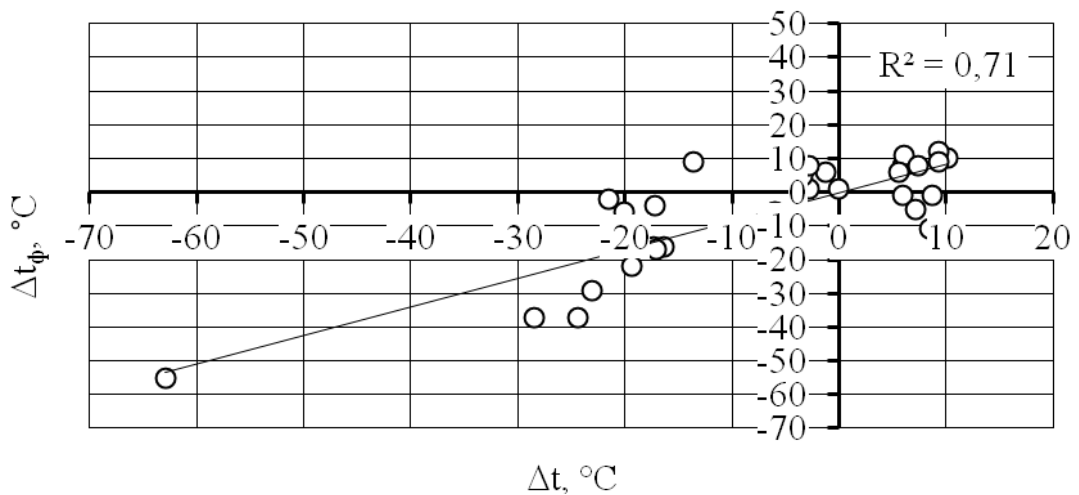


Рис. 5. Диаграмма соответствия рассчитанных и фактических изменений температуры листа между проходами

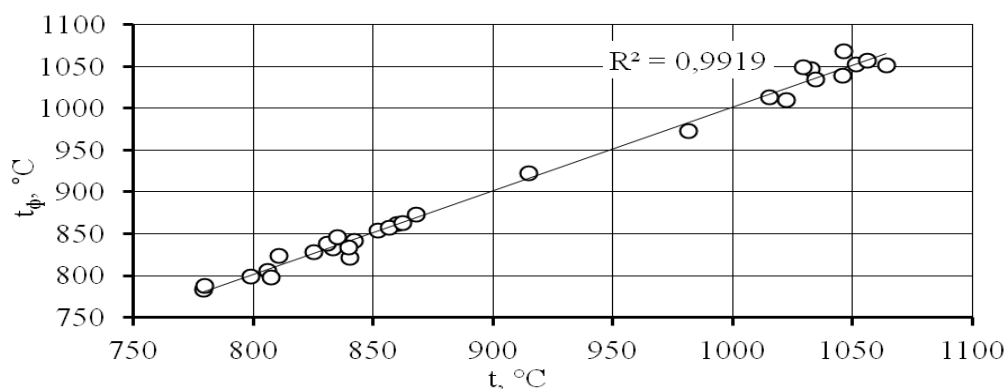


Рис. 6. Диаграмма соответствия рассчитанных и фактических значений температуры начала прокатки в двух последовательных проходах

В применяемых формулах используются следующие параметры:

$R$  – радиус валков, мм;

$t_{wr}$  – температура валков, °С;

$h_0, h_1$  – толщина полосы до и после прохода, мм;

$v_{II}$  – скорость полосы, м/с;

$S'$  – опережение;

$C_{II}$  – теплоемкость полосы, кДж/(м<sup>3</sup>°С):

$$C_{II} = \begin{cases} 422,7 + 48,66 \exp(0,319 \cdot 10^{-5} T), & T \leq 700 \\ 657,0 + 0,084 \left( \frac{T}{1000} \right)^{-24,6}, & T > 700 \end{cases};$$

$\rho_{II} = 7500$  кг/м<sup>3</sup> – плотность полосы;

$\sigma_B$  – временное сопротивление, МПа. Рассчитывается в зависимости от химического состава стали. Для марок СтЗсп, 15ХСНДА, К65 и Х65, получили 450, 470, 470 и 500 МПа соответственно.

#### Библиографический список

1. Румянцев М.И., Белов В.И., Разгулин И.А. Опыт совершенствования методики Л.В.Андреюка для расчета напряжения текучести при горячей листовой прокатке. Электронный журнал «Калибровочное бюро» 5 выпуск, с.73-84, 2015г. URL: [http://passdesign.ru/numbers/number\\_five\\_05\\_2015.zip](http://passdesign.ru/numbers/number_five_05_2015.zip) (дата обращения: 10.02.2016).
2. Коновалов Ю.В., Остапенко А.Л., Пономарев В.И. Расчет параметров листовой прокатки. Справочник. М.: Металлургия, 1986. С.114-162.
3. К вопросу построения модели для расчета составляющих температурного режима металла в линии широкополосного стана горячей прокатки / М.И.Румянцев, И.Г.Шубин, Д.Ю.Загузов, О.С.Носенко // Моделирование и развитие процессов обработки металлов давлением: междунар. сб. науч. тр. Магнитогорск: Изд-во Магнитогорск. гос. техн. ун-та им. Г.И. Носова, 2006. С.26-34.
4. Синтез модели для расчета температуры тонких полос из малоуглеродистых сталей в линии широкополосного стана горячей прокатки / Р.А.Исмагилов, М.И.Румянцев, И.Г.Шубин, и др. // Производство проката. 2007. №5. – С.5-9.
5. Моделирование изменения температуры металла при горячей прокатке толстых полос из низколегированных сталей на широкополосных станах с целью повышения результативности процесса / М.И.Румянцев, И.Г.Шубин, О.Ю.Сергеева и др. // Производство проката. 2009. №9. С.7-11.

**СВЕДЕНИЯ ОБ АВТОРАХ**

**Разгулин Игорь Андреевич** – абитуриент аспирантуры по направлению 22.06.01 «Технология обработки материалов» направленности «Обработка металлов давлением». Тел.: 89634765377. E-mail: igor.darsy@mail.ru.

**Румянцев Михаил Игоревич** – канд. техн. наук, профессор кафедры технологии обработки материалов ФГБОУ ВО «Магнитогорский государственный технический университет им. Г.И. Носова», г.Магнитогорск. Область исследований: совершенствование технологии производства листового проката на основе развития методологии анализа листопрокатных технологических систем. Тел.: 89320139323. E-mail: mihigrum@mail.ru.

**Чикишев Денис Николаевич** – канд. техн. наук, доцент кафедры технологии обработки материалов ФГБОУ ВО «Магнитогорский государственный технический университет им. Г.И. Носова», г.Магнитогорск. Область исследований: создание научных основ получения современных хладостойких и коррозионностойких сталей, их деформационно-термической обработки для достижения уникальных механических и специальных эксплуатационных свойств. Тел.: 89028958755. E-mail: chikishev\_denis@mail.ru.

**Abhary K.** – The University of South Australia.

**Ghomashchi R.** – The University of Adelaide.

**Spuzic Sead** – PhD, MSc, BEng(Hons), Adjunct Senior Research Fellow Division of Information Technology, Engineering and the Environment University of South Australia. Research themes: hot steel rolling, roll pass design, total quality control, knowledge management. Phone: +61883650767; +61883023329. E-mail: Sead.Spuzic@unisa.edu.au.